

Lawrence Berkeley National Laboratory

LBL Publications

Title

De-pollution efficacy of photocatalytic roofing granules

Permalink

<https://escholarship.org/uc/item/96h6m5rv>

Authors

Tang, Xiaochen
Ughetta, Lara
Shannon, Simon K
[et al.](#)

Publication Date

2019-08-01

DOI

10.1016/j.buildenv.2019.03.056

Peer reviewed

1
2
3
4
5
6
7
8
9
10
11
12
13
14
15
16
17
18
19
20
21
22

De-pollution efficacy of photocatalytic roofing granules

Xiaochen Tang¹, Lara Ughetta², Simon K. Shannon², Sébastien Houzé de l’Aulnoit¹,
Sharon Chen¹, Rachael A. T. Gould², Marion L. Russell¹, Jiachen Zhang³, George Ban-Weiss³,
Rebecca L. A. Everman², Frank W. Klink², Ronnen Levinson¹, Hugo Destailats^{1,*}

1. Heat Island Group, Lawrence Berkeley National Laboratory, 1 Cyclotron Road, Berkeley, California 94720, USA.
2. Industrial Mineral Products Division, The 3M Company, 3M Center, Building 209, 1-W-14, St. Paul, Minnesota 55144, USA.
3. Department of Civil and Environmental Engineering, University of Southern California, Los Angeles, California 90089, USA.

* Corresponding author E-mail: HDestailats@lbl.gov

Keywords: asphalt roofing shingle, titanium dioxide, aging, weathering, NO_x, nitrate

23

24 **Abstract**

25 Photocatalytic building surfaces can harness sunlight to reduce urban air pollution. The NO_x
26 abatement capacity of TiO₂-coated granules used in roofing products was evaluated for
27 commercial product development. A laboratory test chamber and ancillary setup were built
28 following conditions prescribed by ISO Standard 22197-1. It was validated by exposing reference
29 P25-coated aluminum plates to a 3 L min⁻¹ air flow enriched in 1 ppm NO under UVA irradiation
30 (360 nm, 11.5 W m⁻²). We characterized prototype granule-surfaced asphalt shingles and loose
31 granules prepared with different TiO₂ loadings and post-treatment formulations. Tests performed
32 at surface temperatures of 25 and 60 °C showed that NO_x abatement was more effective at the
33 higher temperature. Preliminary tests explored the use of 1 ppm NO₂ and of 1 ppm and 0.3 ppm
34 NO/NO₂ mixtures. Specimens were aged in a laboratory accelerated weathering apparatus, and by
35 exposure to the outdoor environment over periods that included dry and rainy seasons. Laboratory
36 aging led to higher NO removal and NO₂ formation rates, and the same catalyst activation was
37 observed after field exposure with frequent precipitation. However, exposure during the dry season
38 reduced the performance. This inactivation was mitigated by cleaning the surface of field-exposed
39 specimens. Doubling the TiO₂ loading led to a 50–150 % increase in NO removal and NO_x
40 deposition rates. Application of different post-treatment coatings decreased NO removal rates (21–
41 35%) and NO_x deposition rates (26–74%) with respect to untreated granules. The mass balance of
42 nitrogenated species was assessed by extracting granules after UV exposure in a 1 ppm NO-
43 enriched atmosphere.

44 1. Introduction

45 Asphalt shingles are the most common residential roofing material in the US (about 80% market
46 share) [1], while asphaltic built-up roofs and modified bitumen membranes are a popular option
47 for low-pitch roofs on commercial buildings [2]. In both products, an impermeable asphaltic layer
48 is surfaced with granules that impart durability and aesthetic properties. Photocatalytic roofing
49 granules have the potential to provide additional environmental benefits by removing commonly
50 found urban atmospheric pollutants such as nitrogen oxides ($\text{NO}_x = \text{NO} + \text{NO}_2$).

51
52 Under sunlight, photo-induced redox chemistry can eliminate soiling and air pollutants adsorbed
53 on the catalyst surface, including organic compounds and atmospheric NO_x [3, 4]. Photocatalytic
54 oxidation enables the removal of NO_x from urban air through their conversion to non-volatile
55 byproducts following the oxidation sequence $\text{NO} \rightarrow \text{NO}_2^- / \text{HNO}_2 \rightarrow \text{NO}_2 \rightarrow \text{NO}_3^- / \text{HNO}_3$ [5, 6].
56 The photocatalytic reaction of NO_x occurring at the TiO_2 surface is prompted by absorption of a
57 UV-A photon (wavelength: 315-400 nm). The final stable oxidation byproducts can be washed off
58 the surface by rain or dew. For that reason, emerging photocatalytic construction materials are
59 specifically designed as *de-noxification* (*de-NO_x*) technologies. Several studies have explored in
60 laboratory tests the initial performance of freshly prepared de- NO_x materials as a function of
61 photocatalyst composition, allotropic form, porosity, microstructure, chemical interactions with
62 substrates (e.g., cement, paint), relative humidity, water content, challenge gas composition, and
63 catalyst loading [7-15]. Fewer studies report the de- NO_x performance of materials that had been
64 aged in contact with the environment. For example, a recent study showed that a photocatalytic
65 coating applied over concrete and plaster maintained about 80% of its initial activity after two
66 years of continuous exposure to polluted urban air [16]. Similarly, a few large-scale field
67 demonstrations of newly installed photocatalytic cementitious materials have been performed,
68 showing disparate results ranging from excellent to poor de- NO_x efficacy [17-24]. The de- NO_x
69 performance can change over time as materials are continuously exposed to the environment
70 because photocatalytic efficacy is influenced by the buildup of recalcitrant residues on the surface
71 (including microbial soiling) and by other physical and chemical changes associated with material
72 aging. For that reason, it is important to evaluate the long-term performance of photocatalytic
73 building materials in contact with the urban environment.

74 Various laboratory test methods have been developed to evaluate the air purification efficacy of
75 photocatalytic materials [25-28]. A widely used approach is ISO Standard 22197-1: “Fine ceramics
76 (advanced ceramics, advanced technical ceramics) – test method for air-purification performance
77 of semiconducting photocatalytic materials. Part 1. Removal of nitric oxide” [29]. This popular
78 method is convenient due to the simplicity of the test chamber and operation conditions, and allows
79 for comparison across several products and materials that have been tested over the years using
80 this standard. However, limitations and shortcomings have been identified, including possible
81 underestimation of uptake rates due to slow diffusion from the gas phase to the catalyst [28, 30,
82 31]. An alternative methodology was proposed as an Italian (UNI) and European (CEN) standard,
83 using a continuously stirred tank photo-reactor [28] to better address those biases. However, this
84 approach may be affected by surface losses and gas-phase reactions due to longer residence times
85 [31].

86
87 All standardized methods are designed to provide quantitative and reliable metrics to compare a
88 wide range of materials. However, their results are not easily applicable to numerical models
89 predicting the impacts on urban air quality of photocatalytic materials operating under real-world
90 conditions. In these tests, photocatalysts are challenged with NO_x concentrations that exceed by
91 one to two orders of magnitude the levels typically found in urban atmospheres (in the range 10 –
92 100 ppb); furthermore, in the case of ISO 22197-1, only NO is used as a reactant. The NO_x removal
93 rate is calculated as the difference between consumed NO and formed NO_2 , assuming that surface-
94 bound nitrate is the only byproduct. However, it is possible that other byproducts besides
95 $\text{HNO}_3/\text{NO}_3^-$ could form during the photocatalytic process. In studies that explored byproduct
96 formation in more detail, N_2O (a greenhouse gas) and nitrous acid (HONO, a reactive species)
97 have been identified as relatively minor byproducts [32-36]. Another study found that HONO
98 efficiently decomposed in contact with irradiated photocatalytic paint, and did not find N_2O [6].
99 Unlike nitrate, which can be effectively scrubbed from the atmosphere, HONO and N_2O may be
100 re-emitted into urban air. Therefore, the mass balance of nitrogen-containing species should be
101 considered to assess the environmental impact of these materials.

102
103 Another limitation of standardized methods is that they are run at ambient room temperature.
104 Under the sunny summer afternoon conditions specified by ASTM Standard E1980-11: “Standard

105 practice for calculating reflectance index of horizontal and low-sloped opaque surfaces” [37], the
106 surface temperature of a well-insulated roof with high thermal emittance (approximately 0.90)
107 ranges from 45 °C if the solar reflectance is 0.80 (bright white color) to 83 °C for an albedo of
108 0.05 (black color). Two opposite effects can be expected to affect the photocatalytic performance
109 at these relatively high roof temperatures, with respect to 25 °C: lower conversion rates due to
110 poorer NO_x adsorption, and an acceleration of the processes due to faster reaction rates. There is
111 little information regarding the effect of increasing surface temperature on the photocatalyzed
112 oxidation of NO_x, and the evidence is not conclusive. One study described faster NO oxidation as
113 temperature rose from 5 to 60 °C [38]. Another study showed that the NO_x removal rate decreased
114 by increasing temperature from 30 °C to 40 °C at low relative humidity, but remained constant at
115 a higher RH setting [39]. A third study observed a reduction in NO removal rates as temperature
116 increased from 20 °C to 30 °C [8].

117

118 This study incorporates several factors to assess the performance of photocatalytic materials under
119 realistic and standardized conditions. A modified version of the experimental approach from ISO
120 22197-1 was adopted to evaluate the photocatalytic performance of prototype granules used in
121 asphalt shingles and modified bitumen roofing membranes. The effect of surface temperature was
122 studied by operating the reactor at 25 °C (per ISO 22197-1) and 60 °C; the latter temperature
123 represents a mid-range value corresponding to a roof albedo of 0.50 and a thermal emittance of
124 0.90. Tests were carried out mostly using 1,000 ppb NO as a challenge gas (per ISO 22197-1).
125 Other conditions were also explored, that included the use of NO₂, an NO/NO₂ mixture, and lower
126 upstream NO_x concentrations. Various granule formulations, which included different catalyst
127 loading and post-treatments, were evaluated as received (unexposed), after accelerated aging in
128 the laboratory, and after aging in the field. Surface-bound nitrate and nitrite were quantified,
129 contributing to closing the mass balance for nitrogen-containing species.

130

131 **2. Experiment**

132 **2.1 Materials**

133 All tested photocatalytic materials were supplied by 3M, except for TiO₂-coated aluminum plates
134 prepared at LBNL for use as reference samples. Two types of photocatalytic roofing materials

135 were tested: (1) loose granules with diameters of about 1 mm and varied surface coatings; and (2)
136 prototype shingle samples prepared by adhering the granules to 10 cm × 20 cm aluminum plates
137 coated with an acrylic layer. Both are illustrated in Figure S1 (Supporting Information). The loose
138 granule samples were used to evaluate the role of different coating formulation parameters and to
139 extract adsorbed species after irradiation. Shingles were used to expose the material to the natural
140 environment and for accelerated aging in the laboratory. Three different groups of photocatalytic
141 roofing materials (A, B, and C) were tested, as described in Table 1. All roofing granules
142 comprised a base mineral core, a pigment coating and a photocatalyst coating. In addition, samples
143 were coated with a proprietary adhesion promoter applied as a post-treatment to help granules stick
144 to the asphalt shingle. Two post-treatment formulations were used, labeled PT1 and PT2, which
145 were two variants of the standard method (STD) that included oil and silicone. Photocatalyst
146 particles were TiO₂ Aeroxide® P25 (Evonik, Germany), except in one case in which TiO₂
147 Aeroxide® P90 (Evonik, Germany) was used in combination with P25 to evaluate the effect of
148 incorporating a different catalyst. The catalyst was dispersed at either a low (1×) or high (2×)
149 loading level through the silicate binder, and applied to the surface of the granules. The silicate
150 binder formed a semi-ceramic coating at the surface of the granules after being fired at 200–370 °C.
151 More details of the granule coating process are provided in two United States patents [40, 41].

152 Group A (shingles) included six different samples: a non-photocatalytic control sample (A0),
153 shingles surfaced with granules prepared with three different types of photocatalytic coatings using
154 the same base mineral and post-treatment PT1 (A1, A2 and A3), and two shingles using granules
155 that incorporated a different post-treatment PT2 (A4 and A5). Multiple specimens were prepared
156 and used for each shingle sample. The solar reflectance of the shingle prototypes ranged 0.12 –
157 0.30 (Table S1, Supporting Information). Group B (loose granules) included six types of white-
158 pigmented samples with different P25 photocatalyst loading. These were further coated with two
159 types of post-treatment formulations (PT1 and PT2), except in two cases that had not been post
160 treated. Group C (loose granules) included four types of samples using a different base mineral,
161 all with white-pigment coating and the same level of P25 photocatalyst coating. Varying levels of
162 silicone in the post-treatment formulations was explored in this group to identify the optimal
163 concentration of this additive. Three duplicate determinations were conducted with identical
164 specimens, validating the consistency among samples and stability of the experimental method.

165 The reference samples were prepared by coating a 10 × 20 cm clean aluminum plate with different
 166 amounts of the P25 catalyst (20.0 mg for 1 g m⁻² surface coverage and 200 mg for 10 g m⁻²)
 167 suspended in 8 mL of de-ionized (DI) water. The suspension was pre-sonicated for 30 minutes to
 168 fully suspend the catalyst in water. After quantitatively transferring the suspension to the surface,
 169 the coated aluminum plate was heated at 60 °C, forming a homogeneous layer after water
 170 evaporated.

171 **Table 1:** Formulation of granule prototypes tested in this study.

Group	Sample	Color	TiO ₂ P25 loading ^a	Post-treatment (PT) ^b
A (granule-surfaced shingles)	A0	White	No TiO ₂ (control)	PT1
	A1	Grey	Low	PT1
	A2	Grey	High ^c	PT1
	A3	White	High	PT1
	A4	White	Low	PT2
	A5	White	High	PT2
B (loose granules)	B1	White	Low	None
	B2	White	High	None
	B3	White	Low	PT1
	B4	White	High	PT1
	B5	White	Low	PT2
	B6	White	High	PT2
C (loose granules)	C1	White	Low	PT1
	C2	White	Low	PT1 without silicone
	C3	White	Low	PT2
	C4	White	Low	Only STD

172
 173 ^a In the range of 0.5 to 1.5 mg of catalyst per g of granules, per references #39 and #40.

174 ^b PT1 and PT2 are two modifications of a standard granule post-treatment using a proprietary
 175 composition (STD).

176 ^c Prepared using a P25 + P90 mixture

177

178 2.2 Aging of shingle samples

179 To evaluate potential changes in performance due to aging, shingle samples from Group A were
180 subjected to accelerated weathering in the laboratory and exposed to the environment (natural
181 aging) in two separate tests.

182 2.2.1 Laboratory aging

183 A sub-set of specimens from samples A1, A2, and A3 was exposed for 1,000 hours in a commercial
184 weathering apparatus (Model QUV/Spray with Solar Eye Irradiance Control, Q-Lab, Westlake OH)
185 following cycle 1 of ASTM Standard G154-12: “Standard practice for operating fluorescent
186 ultraviolet (UV) lamp apparatus for exposure of nonmetallic materials” [42]. This program
187 includes 8 h of ultraviolet (UV) irradiation (at 340 nm) with $0.89 \text{ W m}^{-2} \text{ nm}^{-1}$ intensity at $60 \text{ }^\circ\text{C}$,
188 followed by 4 h water condensation at $50 \text{ }^\circ\text{C}$. At $0.89 \text{ W m}^{-2} \text{ nm}^{-1}$, the instrument delivers an hourly
189 irradiation of 275 kJ m^{-2} . Therefore, exposure in the QUV for 1,000 h is approximately equivalent
190 to 1 year of Florida sunshine (280 MJ m^{-2}) [43].

191 2.2.2 Natural exposure

192 Two separate natural aging exercises were performed on different sub-sets of A samples. In the
193 first case, shingle specimens corresponding to samples A1, A2 and A3 were exposed on racks
194 mounted on a laboratory roof in Berkeley, California (latitude 37.87° N , longitude 122.27° W).
195 Specimens were exposed for about 3 months during the spring and early summer of 2016 (2016-
196 03-25 to 2016-07-11), a dry period during which less than 10 mm of rain was recorded. The
197 maximum hourly average solar irradiance during this time period was 831 W m^{-2} (Table S3).
198 Meteorological data for the city of Berkeley was obtained from the nearby USC00040693 weather
199 station located at the UC Berkeley Campus (approximately 1 km west of the exposure site),
200 belonging to the Global Historical Climatology Network. Specimens for each sample were placed
201 in two south-facing racks tilted at a 45° angle with respect to the floor, as illustrated in Figure S2
202 (Supporting Information). At the end of the exposure period, specimens were retrieved, and their
203 NO_x removal efficacy was analyzed in the laboratory.

204 The second natural exposure test was carried out over a six month period with shingle samples A4
205 and A5, which were installed on 2017-01-13 in the racks tilted at 45° with respect to the horizon.
206 Several identical specimens of each sample were installed side by side and retrieved at different

207 times. Those retrieved on 2017-04-26, after three months of exposure, experienced a rainy winter
208 and early spring, with a total precipitation of 308 mm during that period. By contrast, specimens
209 withdrawn after six months of exposure, on 2017-07-11, had been subsequently exposed to
210 significantly less additional rain (66 mm), which occurred only in the month of April. The
211 cumulative precipitation during the six-month period is presented in Figure S3 (Supporting
212 Information). Average solar irradiance is reported in Table S2 (Supporting Info.). The solar
213 irradiance was weaker in this 6-month period, with a maximum hourly average value of 559 W m^{-2}
214 (Table S3). Specimens retrieved at 3 and 6 months were analyzed in the laboratory to evaluate
215 their NO_x removal efficacy.

216 After determining their de- NO_x performance, specimens retrieved at 6 months were subsequently
217 cleaned in the lab and re-analyzed to assess their regeneration potential. Two cleaning methods
218 were used. In the first (“soft cleaning”) the shingle surface was rinsed four times with 25 mL of
219 de-ionized water using a squirt bottle. In the “hard cleaning” process, the specimen was placed in
220 a beaker filled with de-ionized water and sonicated for 60 min, to facilitate contact between water
221 and occluded materials. Both cleaning operations are illustrated in Figure S4 (Supporting
222 Information).

223

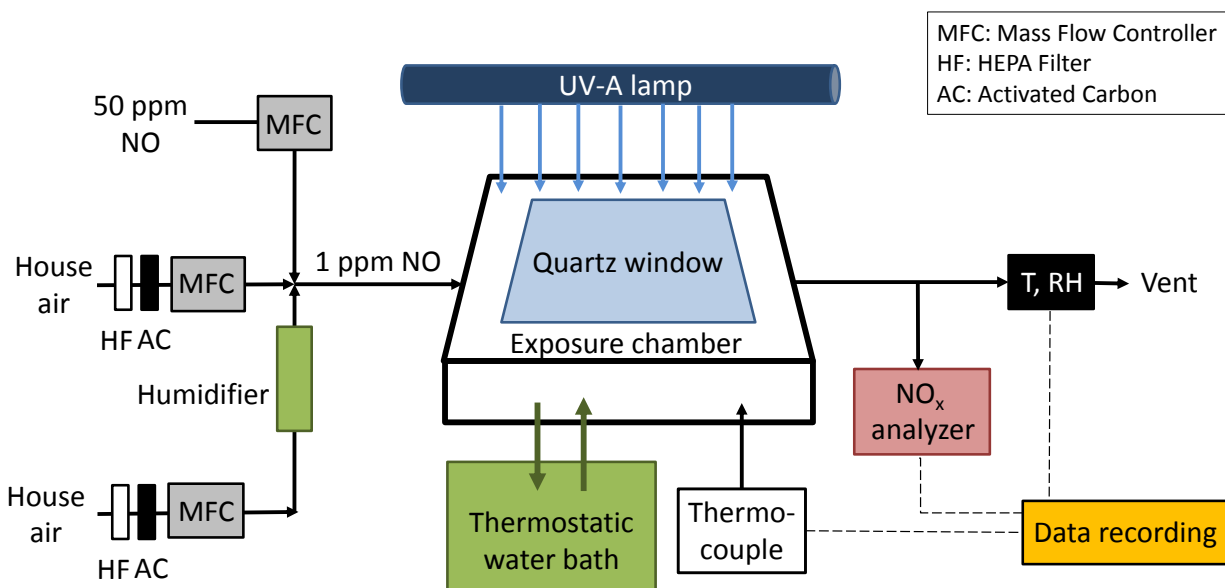
224 **2.3 Evaluation of the photocatalytic performance**

225 *2.3.1 Experimental setup*

226 A bench-scale exposure apparatus and ancillary system was built following conditions stipulated
227 by ISO Standard 22197-1 [29]. The exposure chamber consisted of a flow reactor, UV irradiation
228 source and temperature control using a thermostatic water bath, as illustrated in Figure 1. In each
229 test, a rectangular specimen of 10×20 cm was placed flat at the bottom of the chamber where a
230 quartz window admitted ultraviolet lamplight. The gap between the sample and the window was 5
231 mm. Air enriched with a target concentration of 1,000 ppb NO was introduced upstream at 50%
232 relative humidity (RH) by diluting a 50 ppm NO flow from a pre-mixed cylinder (Praxair, Danbury,
233 CT). In experiments using NO_2 as a challenge gas (by itself or in mixtures with NO), a pre-mixed
234 NO_2 cylinder of 50 ppm was used (Praxair, Danbury, CT). In experiments using upstream
235 concentrations lower than 1,000 ppb, those levels were achieved by reducing the flow delivered

236 by the NO and NO₂ cylinders. Downstream of the system, a chemiluminescent NO_x analyzer
 237 (Model 200A, Teledyne Technologies, Thousand Oaks, CA) was used to record in real time the
 238 concentrations of NO and NO₂ present in the air at the chamber's outlet. The NO_x analyzer was
 239 calibrated at different times during the tests. Three duplicate determinations were conducted with
 240 identical specimens, validating the consistency among samples and stability of the experimental
 241 method.

242



243

244

245 **Figure 1:** Experimental setup following the ISO 22197-1 method with temperature controlling
 246 function.

247

248 Experiments were carried out at room temperature (per ISO 22197-1) and also at a higher
 249 temperature by heating the sample to 60 °C, simulating typical roof temperatures. For the high-
 250 temperature experiments, the chamber base temperature was regulated by circulation of water from
 251 a thermostatic bath using copper tubing embedded in the bottom of chamber. The chamber base
 252 temperature was measured with an inserted thermocouple in good contact with it. Due to its
 253 relatively short residence time (approximately 2 s), the NO-enriched air flowing through the
 254 apparatus was not heated and remained at room temperature. The temperature and relative

255 humidity (RH) of the air exiting the chamber was monitored with an in-line digital T/RH sensor
 256 (HIH6100 series, Honeywell, Morris Plains, NJ) and recorded in real time. The RH was controlled
 257 by splitting the dilution upstream flow, saturating air in one of the lines by circulation through a
 258 water bubbler, and adjusting the relative flow ratios while keeping the total flow rate at 3 L min⁻¹.
 259 Constant UV irradiation at 360 nm (UVA) was provided by a 15 W mercury fluorescent lamp
 260 (Model TL-D, Actinic BL, Philips, Andover, MA). The UV irradiance at 360 nm wavelength was
 261 measured at different points on the specimen's surface with a digital radiometer (Model UVX,
 262 UVP LLC, Upland, CA). The irradiance was highest at the center of the sample and consistent
 263 over the exposed surface, with an average of 11.5 ± 1.5 W m⁻². Irradiance measurements were
 264 performed prior to the beginning of tests and repeated at the end, confirming consistency of the
 265 lamp output over the experimental period.

266 2.3.2 NO_x removal rate and predicted nitrate buildup rate

267 Each individual test comprised three periods in the test chamber:

- 268 a) pre-equilibration of the specimen in the dark with a constant flow of the NO-enriched air;
- 269 b) 4 – 6 h (usually 5 – 6 h) of continuous UV illumination under a constant flow of the NO-
 270 enriched air; and
- 271 c) a final dark period of about 1 h with a constant flow of the NO-enriched air, to verify
 272 restoration of the initial NO levels.

273 Most of the NO reacted in the first 2-3 hours of irradiation, and the phenomenon was fully captured
 274 with a minimum UV exposure of 4 hours. In most tests the irradiation period was 6 hours. The
 275 calculation of NO and NO₂ reaction rates considered the total length of irradiation time. NO
 276 removal rate (r_{NO} , μmol h⁻¹) and NO₂ formation rate (r_{NO_2} , μmol h⁻¹, from oxidation of NO) were
 277 calculated using the difference between the inlet and outlet concentrations of NO and NO₂:

278

$$r_{\text{NO}} = \frac{\int_0^{\tau} n_{\text{NO}_{\text{removed}}}(t) dt}{\tau} = \frac{\int_0^{\tau} [c_{\text{NO}_{\text{in}}}(t) - c_{\text{NO}_{\text{out}}}(t)] dt}{\tau} \times \frac{Q}{V_n} \quad (1)$$

$$r_{\text{NO}_2} = \frac{\int_0^\tau n_{\text{NO}_2\text{formed}}(t) dt}{\tau} = \frac{\int_0^\tau [c_{\text{NO}_2\text{out}}(t) - c_{\text{NO}_2\text{in}}(t)] dt}{\tau} \times \frac{Q}{V_n} \quad (2)$$

279

280 where Q is the air flow rate (L min^{-1}), τ is duration of irradiation (h), t is time (min), n is the
 281 number of moles (mol), c is the concentration in the air ($\mu\text{mol m}^{-3}$), and V_n is the normalized gas
 282 volume for one mole of gas at standard pressure and room temperature (22.4 L). The predicted
 283 maximum nitrate formation rate from oxidation of NO and NO_2 (r_{nitrate} , $\mu\text{mol h}^{-1}$) was determined
 284 from a mass balance, assuming that nitrate and NO_2 are the only byproducts of NO oxidation:

285

$$r_{\text{nitrate}} = r_{\text{NO}} - r_{\text{NO}_2} \quad (3)$$

286

287 This approach provides best-case scenario predictions of the amount of nitrate that can be formed
 288 in the process. The relative yield of NO_2 (Y_{NO_2}) and predicted nitrate yield (Y_{nitrate}) can be
 289 determined as the ratio between their formation rates and the NO reaction rate, as follows:

290

$$Y_{\text{NO}_2} = \frac{r_{\text{NO}_2}}{r_{\text{NO}}} \quad (4)$$

$$Y_{\text{nitrate}} = \frac{r_{\text{nitrate}}}{r_{\text{NO}}} \quad (5)$$

291 Since these are the only two byproducts considered in the analysis, $Y_{\text{NO}_2} + Y_{\text{nitrate}} = 100\%$. The
 292 predicted maximum nitrate buildup rate is reported as the mass of nitrate formed per unit time and
 293 area (in $\text{mg h}^{-1} \text{m}^{-2}$), and the NO_x deposition rate (D_{NO_x}) is calculated as the difference between
 294 NO removal and NO_2 formation rates per unit area (Eq. 6), expressed in moles (in $\mu\text{mol h}^{-1} \text{m}^{-2}$):

295

$$D_{\text{NO}_x} = \frac{r_{\text{NO}} - r_{\text{NO}_2}}{A} \quad (6)$$

296 in which A is the exposed surface area, equal to 0.02 m^2 in all tests. In each experiment, NO loss
297 rate (r_{NO}), NO_2 formation rate (r_{NO_2}), relative yield of NO_2 (Y_{NO_2}) and NO_x deposition rate (D_{NO_x})
298 was calculated following Eqs. (1), (2), (4) and (6), respectively.

299

300 *2.3.3 Extraction and analysis of adsorbed nitrogenated byproducts*

301 After being tested in a regular experiment in which NO-enriched air was flown through the reactor
302 and the sample was irradiated over 6 hours, 5.0 g of the loose granules was extracted in water (ion
303 chromatography grade, Sigma Aldrich) by sonication for 30 minutes. The supernatant was left for
304 at least 48 hours in contact with the granules prior to filtration using $0.22 \mu\text{m}$ pore size syringe
305 filter (Millipore). Another two successive extractions of the same granules were conducted to
306 ensure the maximum amounts of nitrate (NO_3^-) and nitrite (NO_2^-) ions were eluted from the
307 granules. Between each extraction, the supernatant was transferred to a separate volumetric
308 container, and its volume was recorded. The total amount of anion mass detected in the sum of all
309 three extractions was calculated. There was a significant experimental error associated with this
310 method, in the order of 20% (5% from NO_x measurement, 10% from supernatant volume readings,
311 and 5% from distribution of nitrate on granule surfaces).

312 Extracts were analyzed by a Dionex Ion Chromatography System (ICS), model 2000. The ICS is
313 equipped with an autosampler (AS40, Dionex), a hydroxide ion generator (EluGen cartridge,
314 Dionex), a conductivity detector, and an ASRS 300 suppressor. Samples were separated
315 isocratically on an AS11-HC column (Dionex) at 20 mM hydroxide ion and a flow rate of 1.0 mL
316 min^{-1} at $30 \text{ }^\circ\text{C}$. An injection loop of $25 \mu\text{L}$ was used to inject samples. A multi-point calibration
317 ranging from 0.1 mg L^{-1} to 10.0 mg L^{-1} was prepared by diluting a 1.000 g L^{-1} nitrite and nitrate
318 chromatography standard (Sigma Aldrich) and was used to quantify the instrument response. A
319 typical calibration curve has a relative standard deviation of 1.9% and a coefficient of
320 determination of 0.9998. Nitrate and nitrite were quantified in extracts from granules that had been
321 used in the chamber with NO-enriched air. Unexposed granules were also extracted to determine
322 background (blank) values.

323

324 3. Results and Discussion

325 3.1 Validation using a reference photocatalytic sample

326 Prior to carrying out experiments using prototype granules or shingles, the approach was validated
327 by performing tests on P25-coated aluminum plates. The removal rate of NO, formation rate of
328 NO₂, NO₂ yield, NO_x deposition rate and the predicted rate of nitrate buildup were calculated in
329 two separate tests at room temperature using different values of P25 surface coverage, and are
330 reported in Table 2. Figure 2 presents results corresponding to tests using P25 surface coverage of
331 1 g m⁻² (Figure 2-A) and 10 g m⁻² (Figure 2-B). Overall, the NO_x deposition rate and the predicted
332 nitrate buildup rate increased with the catalyst surface coverage, suggesting that the photocatalytic
333 process is limited by the number of available reaction sites. NO_x deposition rates were 18 and 296
334 μmol h⁻¹ m⁻² for P25 surface coverage values of 1 and 10 g m⁻², respectively. These results are
335 consistent with a value of 192 μmol h⁻¹ m⁻² determined using 5 g m⁻² P25 by Mills and Elouali
336 following the same ISO method [30].

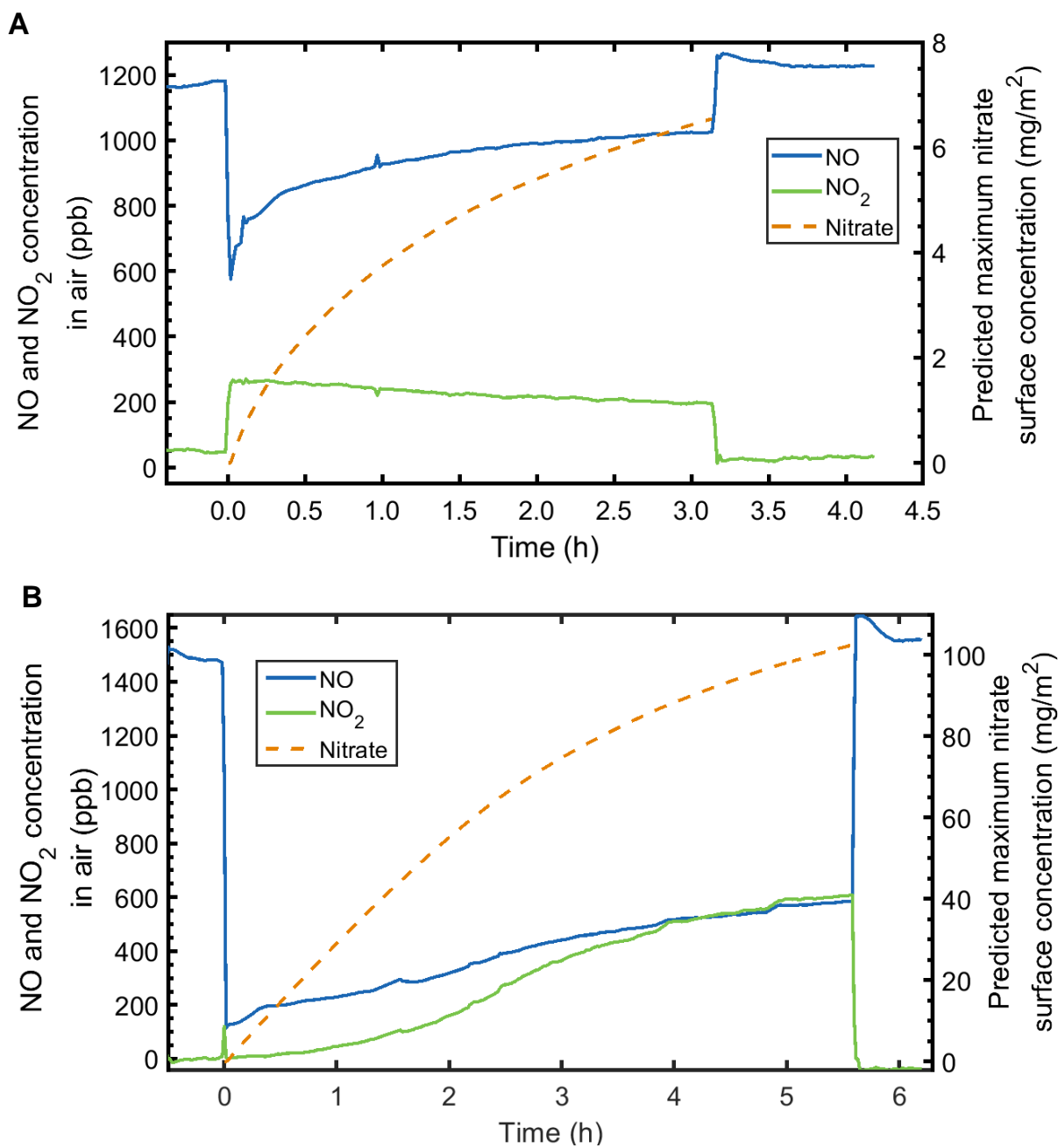
337

338 **Table 2:** Summary of results for P25-coated reference samples and Group A shingle samples.

339

Surface temperature, challenge gas	Sample	UV treatment (h)	NO loss rate, r_{NO} ($\mu\text{mol/h}$)	NO ₂ formation rate, r_{NO_2} ($\mu\text{mol/h}$)	Relative NO ₂ yield, Y_{NO_2} (%)	NO _x deposition rate ($\mu\text{mol/h}\cdot\text{m}^2$)	Predicted maximum nitrate buildup rate ($\text{mg/h}\cdot\text{m}^2$)
P25-coated reference samples							
25 °C 1,000 ppb NO	1 g/m ²	6.0	4.0	3.7	91	18 ±1	1.1 ± 0.1
	10 g/m ²	5.6	8.3	2.4	29	296 ±2	18 ± 0.1
25 °C 1,000 ppb NO ₂	1 g/m ²	6.0	-0.07	-1.3	n.a.	62 ± 1	3.8 ± 0.5
60 °C 1,000 ppb NO	1 g/m ²	6.0	5.2	3.7	72	73 ±2	4.5 ±0.5
60 °C 1,500 ppb NO ₂	1 g/m ²	6.0	-0.4	-1.3	n.a.	47 ±1	2.9 ±0.1
60 °C 1,000 ppb NO/NO ₂	1 g/m ²	6.0	0.96	0.13	n.a.	41±2	2.6 ±0.1
60 °C 300 ppb NO/NO ₂	1 g/m ²	6.0	0.3	-0.1	n.a	21±1	1.3 ±0.03
Unexposed samples							
25 °C 1,000 ppb NO	A1	4.6	0.09	n.d.	n.d.	4.5 ±0.9	0.28 ±0.06
	A2	5.0	0.91	0.43	47	24 ±4	1.5 ±0.2
	A3	4.3	0.19	0.04	22	7 ±2	0.5 ±0.1
60 °C 1,000 ppb NO	A1	5.3	0.08	0.03	36	2.4 ±1.1	0.15 ±0.07
	A2	5.5	2.9	1.3	45	80 ±6	5.0 ±0.4
	A3	5.2	0.28	0.07	24	11 ±1	0.67 ±0.09
	A4	6	0.095	0.062	65	1.6 ±1.0	0.10 ±0.06
	A5	6	0.17	0.071	43	4.7 ±0.8	0.29 ±0.05
Samples exposed to 1000-hour laboratory accelerated aging							
60 °C 1,000 ppb NO	A1	5.3	0.15	0.11	72	2 ±2	0.1 ±0.1
	A2	6.0	2.6	2.2	84	21 ±3	1.3 ±0.2
	A3	6.0	1.7	1.5	87	11 ±1	0.7 ±0.1
Samples exposed to 3 months of natural aging @ 45° tilt angle (2016-03-25 to 2016-07-11)							
60 °C 1000 ppb NO	A1	6.0	0.06	n.d.	n.d.	3 ±2	0.2 ±0.1
	A2	6.0	1.6	1.2	72	23 ±1	1.4 ±0.1
	A3	6.0	0.41	0.28	69	6.3 ±1.3	0.4 ±0.1
Samples exposed to 3 months of natural aging @ 45° tilt angle (2017-01-13 to 2017-04-26)							
60 °C 1,000 ppb NO	A4	6.0	0.73	0.49	67	12 ±2	0.75 ±0.09
	A5	6.0	1.41	1.03	73	19 ±2	1.2 ±0.09
Samples exposed to 6 months of natural aging @ 45° tilt angle (2017-01-13 to 2017-07-11)							
60 °C 1,000 ppb NO	A4	6.0	0.30	0.22	73	4 ±1	0.26 ±0.07
	A5	6.0	0.65	0.52	80	6.7 ±0.6	0.41 ±0.04
Samples cleaned after 6 months of natural aging @ 45° tilt angle							
60 °C 1,000 ppb NO	A4 – soft	6.0	0.24	0.15	64	4.4 ±0.7	0.27 ±0.05
	A4 – hard	6.0	0.38	0.29	78	5 ±1	0.26 ±0.07
	A5 – soft	6.0	0.54	0.33	60	11 ±1	0.68 ±0.09
	A5 – hard	6.0	0.94	0.72	77	12 ±1	0.68 ±0.09

n.a.: does not apply (NO₂ is the reactant); n.d.: not detected



340
 341
 342
 343
 344
 345

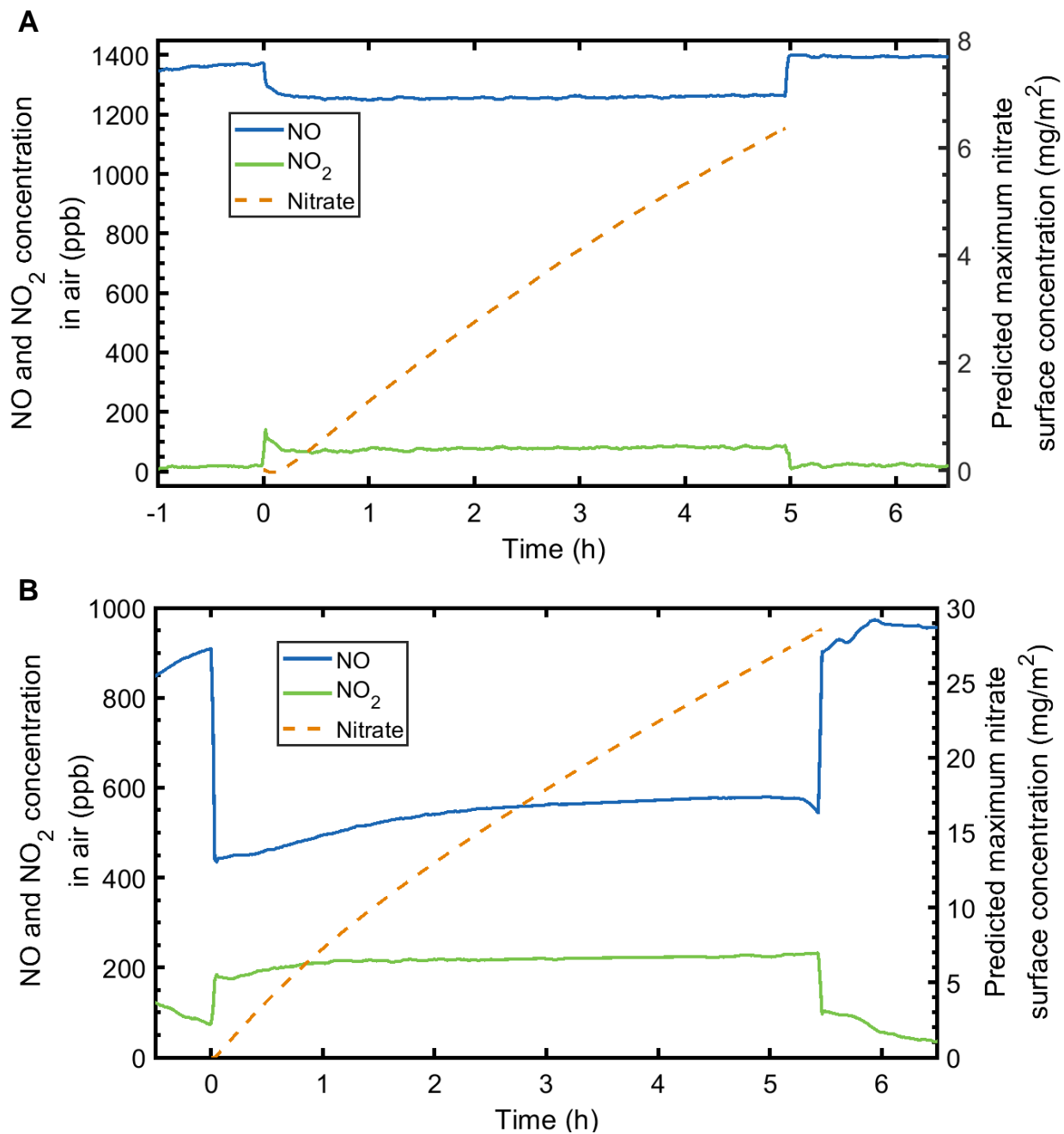
Figure 2: Evolution of NO and NO₂ concentrations during UV irradiation of an aluminum plate coated with (A) 1 g/m² or (B) 10 g/m² of Aeroxide® P25 TiO₂. The predicted maximum concentration of adsorbed nitrate (dashed curve) is reported on the right y-axis.

346 **3.2 Influence of specimen temperature on de-NO_x efficacy**

347 P25 reference (1 g m⁻²) samples and unexposed Group A shingles were tested separately at both
348 25 °C and 60 °C, with all the other experimental parameters remaining the same. Results are
349 presented in Table 2. Curves obtained for shingle sample A2 at both temperatures are shown in
350 Figure 3. Tests carried out at 60 °C showed higher rates for NO oxidation, NO_x deposition and
351 predicted nitrate buildup for the P25 reference sample and for two of the three tested shingle
352 samples with respect to measurements carried out at room temperature. The P25 reference sample
353 had a predicted NO_x deposition rate that was 4 times higher at 60 °C than at 25 °C, while the same
354 parameter for samples A2 and A3 was 3.3 and 1.5 times higher, respectively, at 60 °C than at 25 °C.
355 These results suggest that increasing the surface temperature led to faster photocatalytic reactions,
356 an outcome favorable to the depollution process. Based on these results, it was decided to perform
357 the tests corresponding to sample Groups B and C at 60 °C, better simulating conditions relevant
358 for roofing materials under the sun.

359 These temperature effects can be viewed in the context of a few other studies reporting also the
360 effect of surface temperature on the photocatalytic performance. A study of concrete pavements
361 shows a positive correlation between NO oxidation rates and temperature, with rates tripling as
362 temperature increased from 5 to 60 °C [38]. This result is consistent with the trends reported here.
363 However, a study of photocatalytic stucco coatings found that the NO_x removal rate decreased by
364 increasing temperature from 30 °C to 40 °C when the relative humidity was low (20%), and
365 remained constant for a higher relative humidity of 65%, suggesting that other factors—such as
366 competition for surface sites with moisture and the nature of the substrate—may play a significant
367 role [39]. A study of photocatalytic mortar also showed that increasing temperature from 20 °C to
368 30 °C led to a reduced removal rate for NO [8]. Hence, our results and the limited literature
369 available on the subject suggest that other environmental factors and the nature of the surfaces may
370 affect the temperature dependence of NO_x photocatalytic oxidation. These apparent contradictions
371 should be clarified when more research becomes available.

372



373

374 **Figure 3:** Evolution of NO and NO₂ concentrations during UV irradiation of an unexposed
 375 shingle Sample A2 at (A) room temperature; (B) 60 °C. The predicted maximum concentration
 376 of adsorbed nitrate (dashed curve) is reported on the right y-axis.

377

378

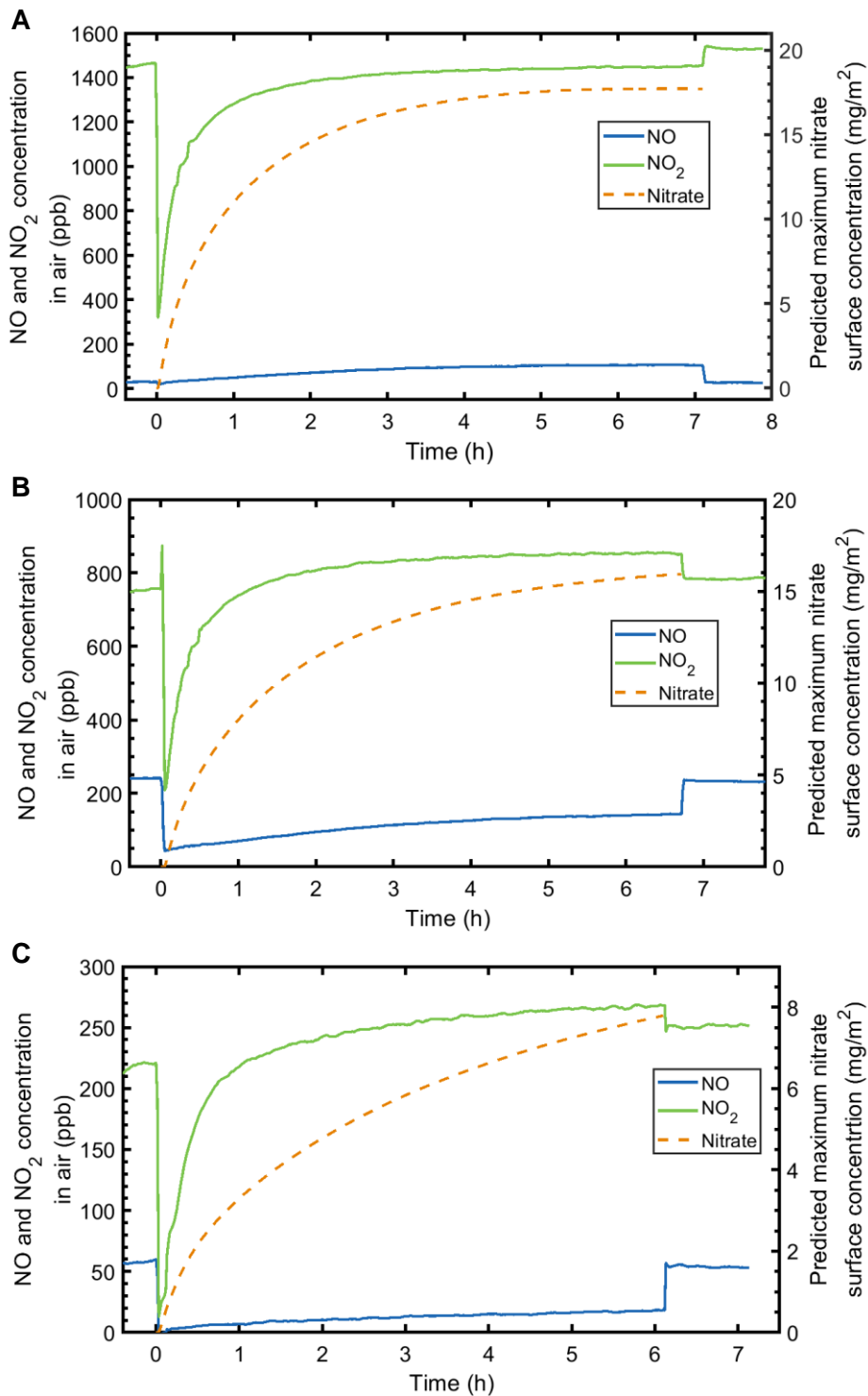
379 3.3 Using NO, NO₂ and NO/NO₂ mixtures as challenge gas

380 In ISO Standard 22197-1, air enriched with 1,000 ppb NO is used to challenge the photocatalytic
381 surface. The same conditions were used in this study. However, in preliminary work we also
382 explored the alternative use of NO₂ and a mixture with a 0.3 NO/NO₂ ratio. The latter is a mixing
383 ratio commonly found in urban air in Los Angeles (see Figure S5 and Table S3, Supporting
384 Information). These additional tests were carried out using P25-coated aluminum plates with 1 g
385 m⁻² catalyst, and results are reported in Table 2. NO₂ was tested at 25 °C (1,000 ppb) and 60 °C
386 (1,500 ppb), while the NO/NO₂ mixture was tested at 60 °C for two total NO_x concentrations of
387 1,000 ppb and 300 ppb. Experimental traces corresponding to these tests are shown in Figure 4.
388 The corresponding formation and removal rates for NO and NO₂, and the NO_x deposition rates,
389 are presented in Figure 5. The difference in removal and formation rates for NO and NO₂ at each
390 temperature determined the extent of NO_x deposition.

391 De-NO_x efficiency of the P25 reference sample was influenced by the challenge gas species and
392 reaction temperature. At 25 °C, the use of NO₂ increased the NO_x deposition rate by a factor of >3,
393 compared with experiments in which the catalyst was exposed to NO. However, the opposite trend
394 was observed at 60 °C: using NO as a challenge gas resulted in a higher NO_x deposition rate than
395 with NO₂. When NO₂ was used as the single challenge gas or as a principal component of the
396 NO/NO₂ mixture, its concentration dropped rapidly during the first few minutes of UV irradiation,
397 consistent with its higher affinity for the TiO₂ surface than that of NO [14, 44]. This initial uptake
398 of NO₂ was followed by a rapid recovery in downstream NO₂ concentration during the initial hour
399 (Figure 4). This behavior is qualitatively different from that observed for NO (Figure 3) and
400 suggests that NO₂ oxidation led primarily to the formation of adsorbed species that partially
401 inactivated the catalyst. When pure NO₂ was used as challenge gas, NO formation was observed,
402 indicating that other chemical processes were taking place in addition to the photooxidation
403 reaction. Those reactions likely involved disproportionation of NO₂ and/or photoreduction of
404 adsorbed nitrate [45-47]. When the NO/NO₂ mixture was used, the final NO₂ concentration at the
405 end of the 6 h irradiation period was higher than the upstream concentration (Figures 4B and 4C),
406 suggesting that a net conversion of NO into NO₂ exceeded the amount of NO₂ being eliminated at
407 the end of the irradiation period. Tests carried out at 300 ppb NO/NO₂ mixture showed a

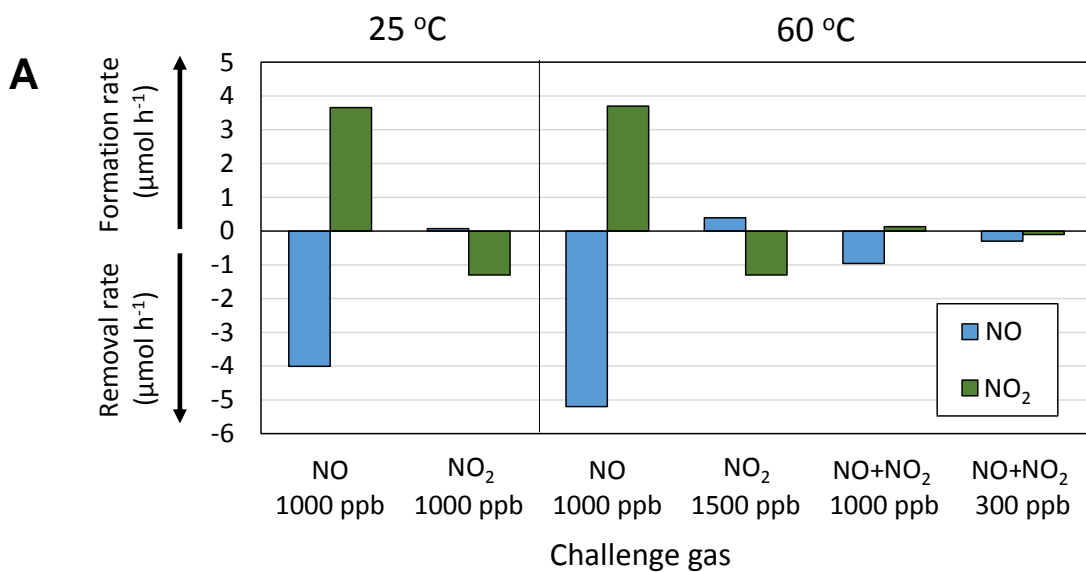
408 proportionally lower NO_x deposition rate than those performed at 1,000 ppb (21 vs. 41 μmol h⁻¹
409 m⁻², respectively).

410 In summary, using different challenge gas had a large effect in the chemical process, the net
411 removal and formation of NO and NO₂, and the NO_x deposition rate. It should be kept in mind that
412 these reaction rates are integrated for 6 h periods during which the relative elimination and
413 formation rates of NO and NO₂ are not constant, further adding to the complexity of this analysis.
414 For that reason, normalized test conditions such as those used in ISO 22197-1 are necessary to
415 provide a meaningful metric.

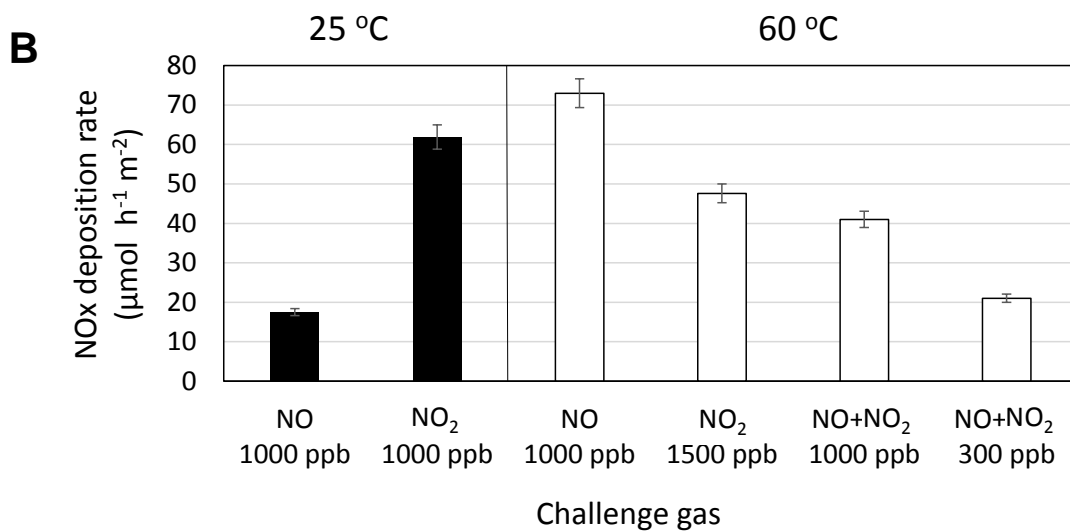


416
 417 **Figure 4.** Experimental traces corresponding to experiments using a P25-coated plated (1 g m^{-2})
 418 at $60 \text{ }^\circ\text{C}$ challenged with (A) NO₂, 1000 ppb; (B) NO/NO₂ = 0.3, 1000 ppb; (C) NO/NO₂ = 0.3,
 419 300 ppb.

420



421



422

423 **Figure 5:** Use of different challenge gases to assess the performance of a reference 1 g/m² P25
424 sample, by measuring (A) removal and formation rates for NO and NO₂; (B) NO_x deposition
425 rate.

426

427 **3.4 Influence of material aging on de-NO_x efficacy**

428 The results for the fresh (unexposed) and aged samples corresponding to Group A are summarized
429 in Table 2. In all cases, the performance was evaluated with a 1,000 ppm NO challenge, at 60 °C.
430 Figures 6 and 7 show the reaction rates and relative yield of NO₂ and nitrate formation for the
431 unexposed materials and for shingles aged under different conditions. Both laboratory aging and
432 field exposure were found to induce changes in the photocatalytic activity of the shingle samples,
433 reflected in variations not only of the NO and NO₂ reaction rate, but also of the NO_x deposition
434 rate and the predicted maximum nitrate buildup rate.

435 *3.4.1 Laboratory aging*

436 Exposure of specimens in the laboratory weathering apparatus led, in most cases, to an increase in
437 NO removal and NO₂ formation rates, as compared with unexposed samples. Such activation of
438 the photocatalyst did not necessarily translate into higher NO_x deposition rates, because most of
439 the additional NO consumed was converted into NO₂, with a net zero NO_x balance (Figure 6).

440 *3.4.2 Field exposure*

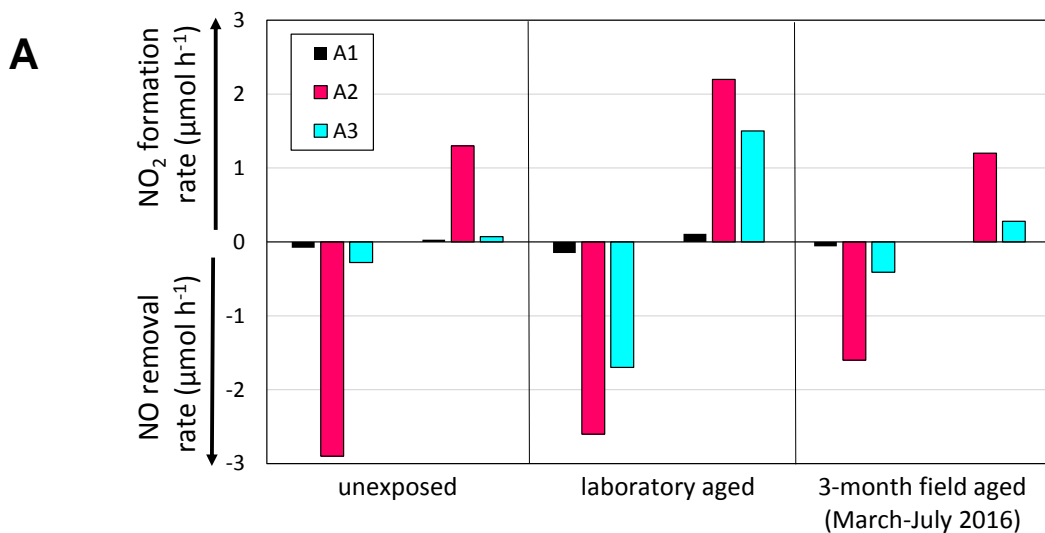
441 Two sets of shingles were exposed in the field during different periods. In the first case, three
442 months of natural aging reduced the photocatalytic activity of samples A1 and A2, but sample A3
443 was not influenced by aging. The NO_x removal efficiency was reduced for all three samples (Figure
444 6). This result is consistent with catalyst inactivation and partial blockage of active sites by
445 particulate matter and other atmospheric chemicals deposited on the surface. It should be noted
446 that the exposure period was fully within the dry season in Northern California. The lack of
447 precipitation likely contributed to soiling buildup and catalyst inactivation.

448 By contrast, the second set of shingles (A4 and A5) was exposed during the rainy season during
449 the initial three months, followed by another three months capturing the dry season (Figure 7).
450 Both samples were strongly activated during the rainy season, and the activity decreased after the
451 second period. The NO_x deposition rate increased significantly during the rainy season, but it
452 dropped back to levels similar to those recorded for the unexposed samples at the end of the six-
453 month period. Specimens that were exposed for six months were subsequently cleaned in the
454 laboratory using two different protocols. A simple rinsing of the surface (“soft cleaning”) slightly
455 reduced both the NO removal and NO₂ formation rates but increased the NO_x deposition rates for

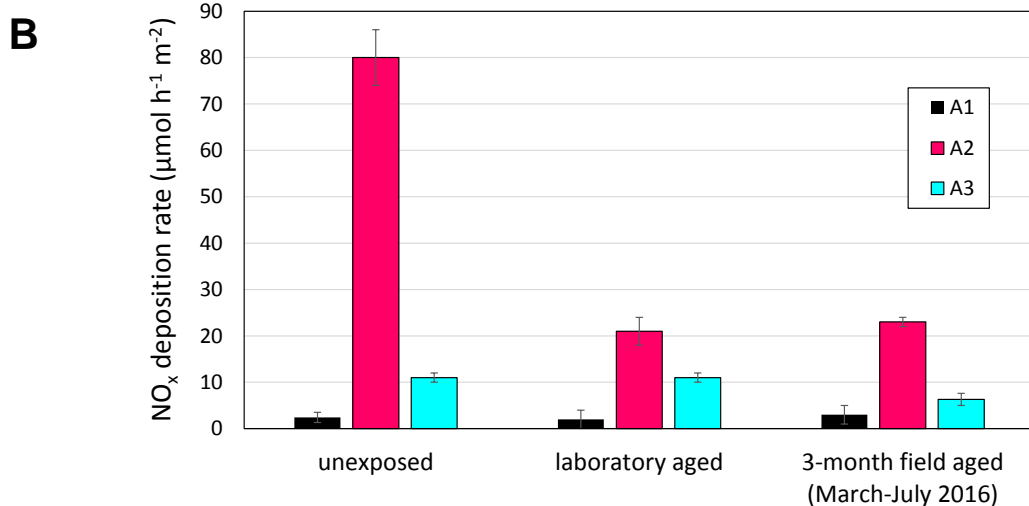
456 samples A4 and A5 by 10% and 64%, respectively. The more energetic (“hard”) cleaning using an
457 ultrasonic bath led to higher NO and NO₂ rates, also with a higher NO_x deposition rate in the case
458 of samples A4 (25%) and A5 (79%). The changes observed during dry and rainy periods, and the
459 partial recovery of the activity due to surface cleaning, support the hypothesis that the
460 accumulation of surface species partially blocking the catalyst can be mitigated by dissolution of
461 water-soluble species (including nitrate), combined with physical removal. This observation is
462 consistent with that of Lettieri et al. [24] showing that photodegradation efficiency of TiO₂-coated
463 limestone decreased after eight months of exposure in the field, which was partially recovered
464 after washing the sample surface with water. The deactivation of TiO₂ catalyst may be caused by
465 the loss of TiO₂ nanoparticles, as well as blockage of active photocatalytic sites as a result of
466 contaminant degradation intermediates and byproducts [48].

467

468

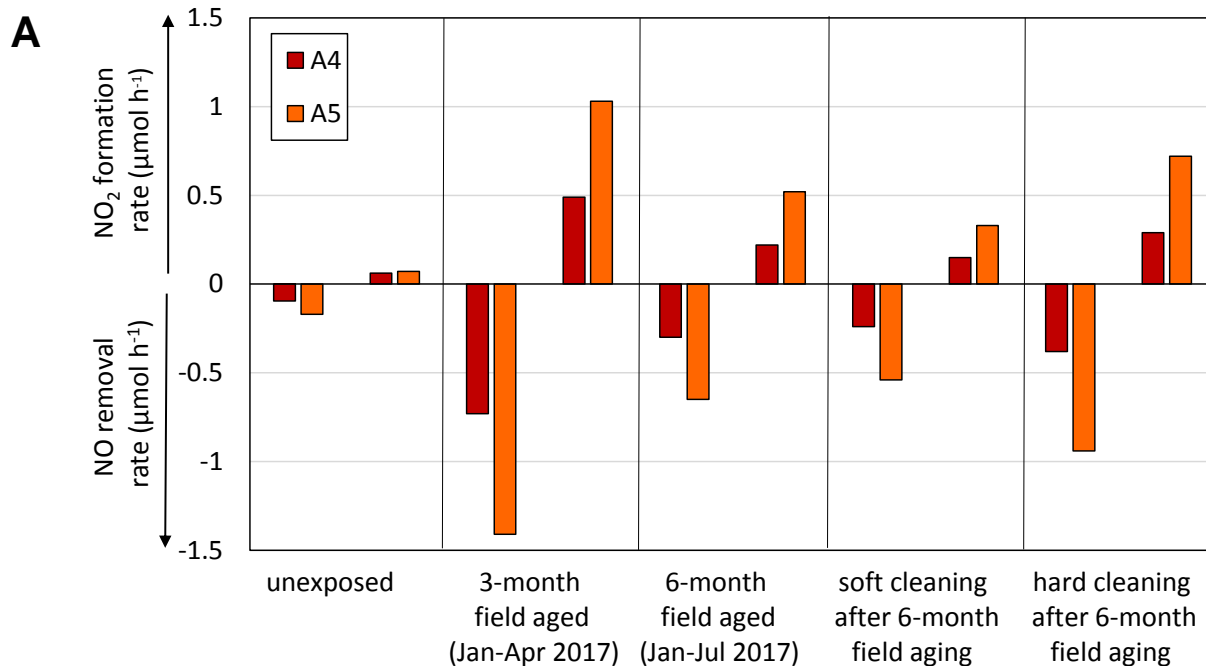


469

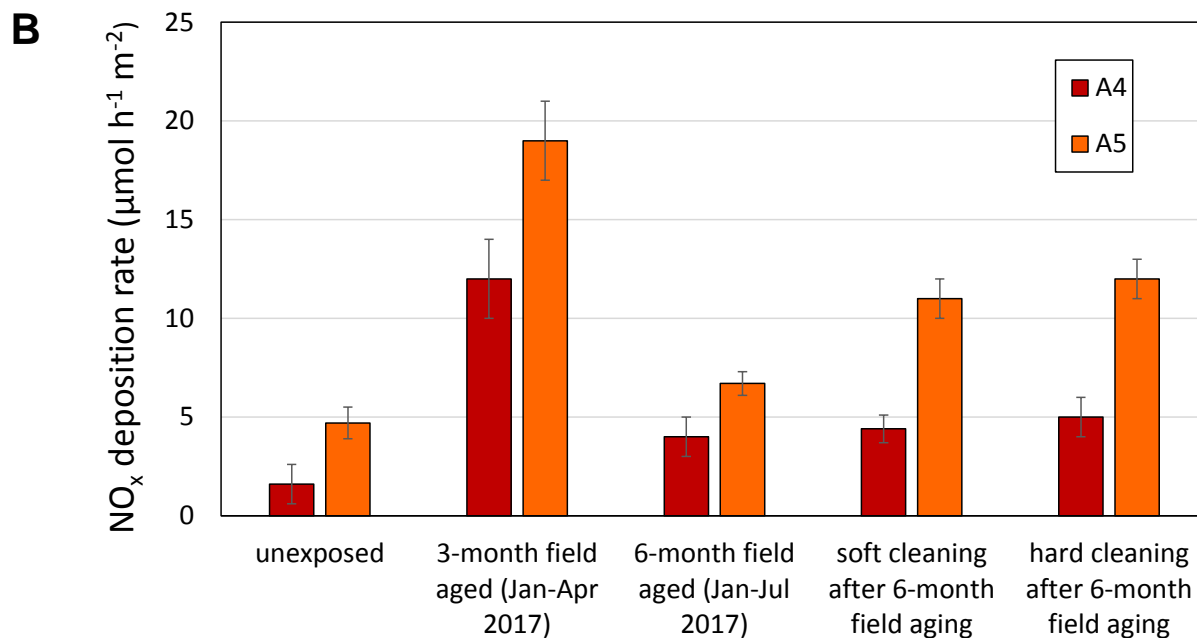


470

471 **Figure 6:** Comparison of (A) reaction rates and (B) NO_x deposition rates determined for three
472 shingle samples prior to exposure, after laboratory aging and after three months of exposure in the
473 field during the dry season. Tests were carried out with a challenge of 1,000 ppb NO at 60 °C.



474



475

476 **Figure 7:** Comparison of (A) reaction rates and (B) NO_x deposition rates determined for two
 477 shingle samples under different conditions. Tests were carried out with a challenge of 1000 ppb
 478 NO at 60 °C.

479 **3.5 Influence of granule coating formulations**

480 Photocatalyst loading and the application of different post treatment coatings influenced the de-
481 polluting capabilities of shingle and loose granule samples. Shingles with more photocatalyst
482 outperformed corresponding samples with the same post-treatment and a lower P25 loading (e.g.,
483 A3 > A1 and A5 > A4). In the case of sample A2, the presence of a different type of catalyst (P90)
484 in combination with P25 led to increased activity. The non-photocatalytic control sample A0
485 showed no de-NO_x activity.

486 The combined effect of the photocatalyst loading and different post treatments was further
487 examined with Group B granule samples (Table 3). While the irradiation duration for samples B2
488 and B3 was different than that for B1, most NO reacted in the first 2-3 h, thus the illumination
489 duration did not have a major impact on the determined parameters. Samples with the higher
490 photocatalyst loading per mass of granule showed higher NO_x removal capacity than those with a
491 lower loading. Similar to the above described results for Group A, doubling the photocatalyst
492 loading led to a proportional increase of 50–100 % in the NO reaction rate and the NO_x deposition
493 rates. Comparing granules with the same photocatalyst loading, those with PT1 (B3) and PT2 (B5)
494 showed lower performance than a similar sample without post-treatment (B1). Comparing samples
495 with the lower P25 loading, the NO removal rates were 14% (B3) and 6% (B4) of the value
496 determined for B1. Similarly, for the same samples the NO_x deposition rate was 28% (B3) and 6%
497 (B5) with respect to B1. The same analysis applied to samples with the higher P25 loading showed
498 that NO removal rates for post-treated samples were 12% (B4) and 5% (B6) the value
499 corresponding to B2, and the NO_x deposition rates were 26% (B4) and 8% (B6) those of B2.

500 The potential influence of silicone used in post-treatment formulations was evaluated with Group
501 C loose granules (Table 3). While the potential deactivation of TiO₂ active sites by siloxanes is
502 well documented [49, 50], there was no significant reduction in the photocatalytic activity caused
503 by the presence of silicone. The differences observed are of the same magnitude as the
504 experimental error; additional studies will be needed to better assess the role of silicone.

505

506 **Table 3:** Experimental results for Group B and Group C loose granule samples.

Challenge NO concentration (ppb)	Sample	TiO ₂ P25 loading	Post treatment ^a	UV treatment (h)	NO loss rate, r_{NO} ($\mu\text{mol/h}$)	NO ₂ formation rate, r_{NO_2} ($\mu\text{mol/h}$)	Relative NO ₂ yield, Y_{NO_2} (%)	NO _x deposition rate ($\mu\text{mol/h}\cdot\text{m}^2$)	Predicted maximum nitrate buildup rate ($\text{mg/h}\cdot\text{m}^2$)
1,000	B1	Low	–	6	1.8	1.2	68	29 ±1	1.8 ±0.1
1,000	B2	High	–	4.4	3.3	2.1	65	58 ±2	3.6 ±0.2
760 ^b	B3	Low	PT1	5.1	0.25	0.09	35	8.0 ±0.6	0.50 ±0.04
1,000	B4	High	PT1	6	0.41	0.11	26	15 ±1	0.93 ±0.05
1000	B5 ^c	Low	PT2	6	0.10	0.06	65	1.6 ±1.0	0.1 ±0.06
1000	B6 ^c	High	PT2	6	0.17	0.07	43	4.7 ±0.8	0.29 ±0.05
1,000	C1	Low	PT1	6	1.7	0.43	25	65 ±19	4.1 ±1.2
1,000	C2	Low	PT1 w/o silicone	6	1.5	0.33	22	59 ±8.2	3.6 ±0.5
1,000	C3	Low	PT2	6	1.4	0.36	26	52 ±6.6	3.2 ±0.4
1,000	C4	Low	Only STD	6	1.9	0.41	22	72 ±5.9	4.5 ±0.4

507 ^a PT1 and PT2 are two modifications of a standard granule post-treatment using a proprietary composition (STD).

508 ^b Slightly lower challenge NO concentration was used due to lower MFC setting.

509 ^c Shingle sample instead of loose granule sample was used in the experiment.

510

511 **3.6 Mass balance of nitrogenated species**

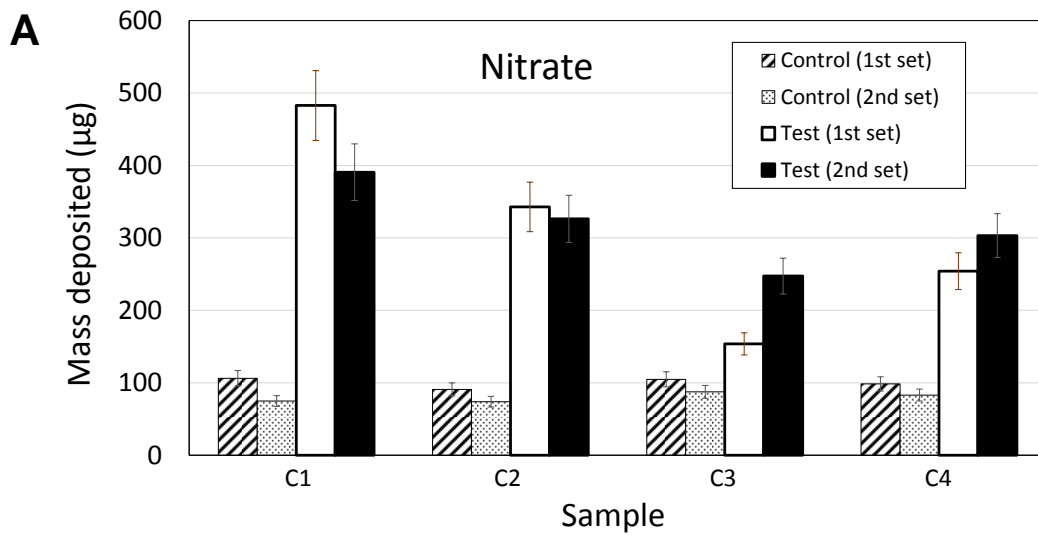
512 In the experiments reported in Tables 2 and 3, the calculation of maximum nitrate buildup rate
513 assumed that no other nitrogenated species were formed and that nitrate anions remained on the
514 surface. This hypothesis was evaluated by extracting four different loose granule samples from
515 Group C that had previously been exposed to NO-enriched air as described in Section 2.3.3.
516 Unexposed granules from the same samples were also extracted, as a reference. The mass of nitrate
517 and nitrite anions determined for each sample (in duplicate determinations) is reported in Figure
518 8. These values were determined from the sum of three subsequent extractions, with the first
519 extract containing more than 90% of the total amount (as illustrated in Figure S6, Supporting
520 Information). The mass of nitrate deposited in samples that had been exposed to NO under UV
521 irradiation was in the range 150 – 480 μg . There was a non-negligible amount of nitrate present in
522 the unexposed granules (75 – 105 μg), which was in all cases lower than the amount found in
523 exposed granules. By contrast, very low levels of nitrite were observed, in the order of 1% of the
524 nitrate mass. While nitrate results show good consistency between each pair of duplicate
525 determinations, the nitrite data is much more scattered because reported levels were close to the
526 limit of quantification.

527 The difference between NO-exposed and unexposed granules can be attributed to the formation of
528 nitrate during the photocatalytic process. The amount of nitrate formed was compared with the
529 predicted maximum mass calculated based on the NO_x deposited in a sample surface of 0.02 m^2 .
530 Overall, the amount of nitrate measured in the extracted samples was 42 – 69% of the predicted
531 maximum nitrate mass for those samples. These quantities account for a large fraction of the
532 expected nitrate recoveries in the extraction, but were below the predicted maximum values. This
533 result is in line with a recent report by Mothes et al. [14], in which mass closure of nitrogenated
534 species in a comparable experiment was achieved only when a relatively low amount of NO_x was
535 removed (<25 μmol per m^2 of photocatalytic surface), and nitrate yields below 100% were
536 observed when a higher amount of NO_x was removed. Our tests, with 75 – 325 μmol NO_x removed
537 per m^2 of exposed granule surface, were comparable with the lower nitrate yield tests reported by
538 Mothes et al. [14]. There are at least three possible explanations for the partial loss of nitrate in the
539 extracted samples:

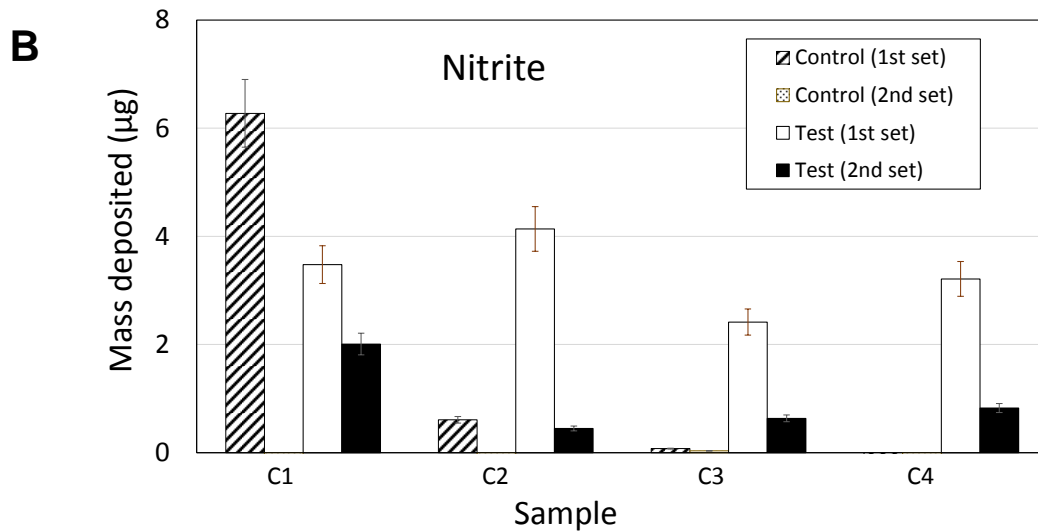
- 540 1) not all nitrate present in the material was extracted, with a fraction remaining strongly
541 attached to the granules, possibly inside pores;
- 542 2) nitrate formed during the photocatalytic process may be partially adsorbed to chamber
543 surfaces, and thus not extracted from the granules; and
- 544 3) other nitrogenated species, such as HNO_3 , HONO or N_2O , may form during the
545 photocatalytic process and be released to the gas phase [5, 32, 34].

546 Considering the very low levels of nitrite observed in the extracts, we do not expect high
547 HONO concentrations in chamber air. Irreversible nitrate uptake in the bulk of granules and
548 losses to reactor walls are likely the main reasons for the discrepancies between predicted and
549 measured surface-bound nitrate. Even if low levels of HONO or N_2O were formed in the
550 photocatalytic process, those contributions would likely be negligible compared with other
551 naturally occurring sources of those species.

552



553



554

555

556

557 **Figure 8:** Mass of (A) nitrate and (B) nitrite ion determined in the first extraction of two sets of
 558 loose granules.

559

560 **4. Summary**

561 The tested photocatalytic materials showed significant NO_x abatement activity, and can contribute
562 to atmospheric de-noxification by oxidizing NO and NO₂ to adsorbed nitrate anions that can
563 subsequently be washed away from the surface. Their performance was affected by key parameters
564 such as the granule coating formulation, surface temperature and aging conditions.

565 Granule post-treatments applied over the TiO₂ coating, which are required to improve adhesion to
566 the substrate, led to decreased photocatalytic performance. This study could not associate this
567 partial inactivation to the presence of silicone in post-treatment formulations, despite suggestions
568 to the contrary in the literature.

569 Evaluation of photocatalytic performance at room temperature, as specified by ISO Standard
570 22197-1, might underestimate the performance of building envelope materials, since their
571 temperature is significantly higher under direct sunlight, and this study reports significantly better
572 performance at 60 °C than at 25 °C. Variation of the ISO standard method using not only NO as
573 the challenge gas but NO₂ or NO/ NO₂ mixture was also investigated, confirming the sensitivity
574 of experimental results to the challenge gas composition.

575 The assessment of the effects of sample aging in the outdoor environment suggests potential
576 performance enhancement by activation with solar irradiation and precipitation, as well as
577 deactivation as a result of soiling, and possible catalyst inactivation. Experiments with specimens
578 that were cleaned in the laboratory after environmental exposure showed also that the partial
579 inactivation can be reversible.

580 This study provided only limited insight on the effect of aging, which is a function of location,
581 climate and duration of exposure. A comprehensive testing plan spanning several years of
582 exposure in multiple locations would be required to more completely assess aged performance.

583 Future work could advance this field by evaluating the performance of photocatalytic granulated
584 roofing materials in large-scale demonstrations. Such studies could provide valuable insights on
585 the impacts of the de-NO_x chemistry in the proximity of treated buildings, such as on street canyons
586 where city dwellers are primarily exposed to urban pollution.

587

588 **Acknowledgements**

589 This research was funded by the Industrial Mineral Products Division of the 3M Company under
590 contract FP00002421. Lawrence Berkeley National Laboratory operates under U.S. Department
591 of Energy Contract DE-AC02-05CH11231.

592

593 **References**

594 [1] R.M. Levinson, S.S. Chen, G.A. Ban-Weiss, H.E. Gilbert, P.H. Berdahl, P.J. Rosado, H.
595 Destailats, M. Sleiman, T.W. Kirchstetter, Next-generation factory-produced cool asphalt
596 shingles: Phase 1 final report, LBNL Report 2001007, (2016) Lawrence Berkeley National
597 Laboratory, Berkeley, CA. <http://escholarship.org/uc/item/2t3602nt>.

598 [2] L. Picone, Asphalt low-sloped roofing: Enduring the test of time?, RCI Interface, September
599 (2009) <http://rci-online.org/wp-content/uploads/2009-2009-picone.pdf>.

600 [3] M.R. Hoffmann, S.T. Martin, W.Y. Choi, D.W. Bahnemann, Environmental Applications Of
601 Semiconductor Photocatalysis, Chem Rev, 95 (1995) 69-96. <https://doi.org/10.1021/cr00033a004>

602 [4] O. Carp, C.L. Huisman, A. Reller, Photoinduced reactivity of titanium dioxide, Prog Solid
603 State Ch, 32 (2004) 33-177. <https://doi.org/10.1016/j.progsolidstchem.2004.08.001>

604 [5] S. Devahasdin, C. Fan Jr, K. Li, D.H. Chen, TiO₂ photocatalytic oxidation of nitric oxide:
605 transient behavior and reaction kinetics, Journal of Photochemistry and Photobiology A:
606 Chemistry, 156 (2003) 161-170. [https://doi.org/10.1016/S1010-6030\(03\)00005-4](https://doi.org/10.1016/S1010-6030(03)00005-4)

607 [6] S. Laufs, G. Burgeth, W. Duttlinger, R. Kurtenbach, M. Maban, C. Thomas, P. Wiesen, J.
608 Kleffmann, Conversion of nitrogen oxides on commercial photocatalytic dispersion paints,
609 Atmospheric Environment, 44 (2010) 2341-2349. <http://doi.org/10.1016/j.atmosenv.2010.03.038>

610 [7] J. Angelo, L. Andrade, A. Mendes, Highly active photocatalytic paint for NO_x abatement under
611 real-outdoor conditions, Applied Catalysis A: General, 484 (2014) 17-25.
612 <http://dx.doi.org/10.1016/j.apcata.2014.07.005>

- 613 [8] N. Bengtsson, M. Castellote, Photocatalytic Activity for NO Degradation by Construction
614 Materials: Parametric Study and Multivariable Correlations, *Journal of Advanced Oxidation*
615 *Technologies*, 13 (2010) 341-349. <http://dx.doi.org/10.1515/jaots-2010-0311>
- 616 [9] J.Z. Bloh, A. Folli, D.E. Macphee, Photocatalytic NO_x abatement: why the selectivity matters,
617 *RSC Advances*, 4 (2014) 45726-45733. <http://doi.org/10.1039/c4ra07916g>
- 618 [10] A. Folli, C. Pade, T.B. Hansen, T. De Marco, D.E. Macphee, TiO₂ photocatalysis in
619 cementitious systems: Insights into self-cleaning and depollution chemistry, *Cement and Concrete*
620 *Research*, 42 (2012) 539-548. <http://doi.org/10.1016/j.cemconres.2011.12.001>
- 621 [11] M. Horgnies, I. Dubois-Brugger, E.M. Gartner, NO_x de-pollution by hardened concrete and
622 the influence of activated charcoal additions, *Cement and Concrete Research*, 42 (2012) 1348-
623 1355. <http://doi.org/10.1016/j.cemconres.2012.06.007>
- 624 [12] R. Sugraney, J.I. Alvarez, M. Cruz-Yusta, I. Marmol, J. Morales, J. Vila, L. Sanchez,
625 Enhanced photocatalytic degradation of NO_x gases by regulating the microstructure of mortar
626 cement modified with titanium dioxide, *Building And Environment*, 69 (2013) 55-63.
627 <http://dx.doi.org/10.1016/j.buildenv.2013.07.014>
- 628 [13] L. Yang, A. Hakki, F. Wang, D.E. Macphee, Different roles of water in photocatalytic DeNO_x
629 mechanisms on TiO₂: Basis for engineering nitrate selectivity, *ACS Appl. Mater. Interfaces*, 9
630 (2017) 17034-17041. <http://doi.org/10.1021/acsami.7b01989>
- 631 [14] F. Mothes, S. Ifang, M. Gallus, B. Golly, A. Boreave, R. Kurtenbach, J. Kleffmann, C. George,
632 H. Herrmann, Bed flow photoreactor experiments to assess the photocatalytic nitrogen oxides
633 abatement under simulated atmospheric conditions, *Applied Catalysis B: Environmental*, 231
634 (2018) 161-172. <http://doi.org/10.1016/j.apcatb.2018.03.010>
- 635 [15] L. Yang, A. Hakki, F. Wang, D.E. Macphee, Photocatalyst efficiencies in concrete technology:
636 The effect of photocatalyst placement, *Applied Catalysis B: Environmental*, 222 (2018) 200-208.
637 <http://doi.org/10.1016/j.apcatb.2017.10.013>

- 638 [16] R. Zouzelka, J. Rathousky, Photocatalytic abatement of NO_x pollutants in the air using
639 commercial functional coating with porous morphology, *Applied Catalysis B: Environmental*, 217
640 (2017) 466-476. <http://dx.doi.org/10.1016/j.apcatb.2017.06.009>
- 641 [17] M. Gallus, V. Akylas, F. Barmpas, A. Beeldens, E. Boonen, A. Boreave, M. Cazaunau, H.
642 Chen, V. Daele, J.F. Doussin, Y. Dupart, C. Gaimoz, C. George, B. Grosselin, H. Herrmann, S.
643 Ifang, R. Kurtenbach, M. Maille, A. Mellouki, K. Miet, F. Mothes, N. Moussiopoulos, L. Poulain,
644 R. Rabe, P. Zapf, J. Kleffmann, Photocatalytic de-pollution in the Leopold II tunnel in Brussels:
645 NO_x abatement results, *Building And Environment*, 84 (2015) 125-133.
646 <https://doi.org/10.1016/j.buildenv.2014.10.032>
- 647 [18] M. Gallus, R. Ciuraru, F. Mothes, V. Akylas, F. Barmpas, A. Beeldens, F. Bernard, E. Boonen,
648 A. Boreave, M. Cazaunau, N. Charbonnel, H. Chen, V. Daele, Y. Dupart, C. Gaimoz, B. Grosselin,
649 H. Herrmann, S. Ifang, R. Kurtenbach, M. Maille, I. Marjanovic, V. Michoud, A. Mellouki, K.
650 Miet, N. Moussiopoulos, L. Poulain, P. Zapf, C. George, J.F. Doussin, J. Kleffmann,
651 Photocatalytic abatement results from a model street canyon, *Environ. Sci. Pollut. Res.*, 22 (2015)
652 18185-18196. <https://doi.org/10.1007/s11356-015-4926-4>
- 653 [19] A. Folli, M. Strom, T.P. Madsen, T. Henriksen, J. Lang, J. Emenius, T. Klevebrant, A. Nilsson,
654 Field study of air purifying paving elements containing TiO₂, *Atmospheric Environment*, 107
655 (2015) 44-51. <http://dx.doi.org/10.1016/j.atmosenv.2015.02.025>
- 656 [20] M.M. Ballari, H.J.H. Brouwers, Full scale demonstration of air-purifying pavement, *J Hazard*
657 *Mater*, 254 (2013) 406-414. <http://dx.doi.org/10.1016/j.jhazmat.2013.02.012>
- 658 [21] E. Boonen, A. Beeldens, Recent Photocatalytic Applications for Air Purification in Belgium,
659 *Coatings*, 4 (2014) 553-573. <http://doi.org/10.3390/coatings4030553>
- 660 [22] C.J. Cros, A.L. Terpeluk, L.E. Burriss, N.E. Crain, R.L. Corsi, M.C.G. Juenger, Effect of
661 weathering and traffic exposure on removal of nitrogen oxides by photocatalytic coatings on
662 roadside concrete structures, *Mater. Struct.*, 48 (2015) 3159-3171. [http://doi.org/10.1617/s11527-](http://doi.org/10.1617/s11527-014-0388-2)
663 014-0388-2

- 664 [23] C. George, A. Beeldens, F. Barmpas, J.F. Doussin, G. Manganelli, H. Herrmann, J. Kleffmann,
665 A. Mellouki, Impact of photocatalytic remediation of pollutants on urban air quality, *Front.*
666 *Environ. Sci. Eng.*, 10(5) (2016) 1-11. <http://doi.org/10.1007/s11783-016-0834-1>
- 667 [24] M. Lettieri, D. Colangiuli, M. Masieri, A. Calia, Field performances of nanosized TiO₂ coated
668 limestone for a self-cleaning building surface in an urban environment, *Building and Environment*,
669 147 (2019) 506-516. <https://doi.org/10.1016/j.buildenv.2018.10.037>
- 670 [25] K. Amrhein, D. Stephan, Principles and test methods for the determination of the activity of
671 photocatalytic materials and their application to modified building materials, *Photochem.*
672 *Photobiol. Sci.*, 10 (2011) 338-342. <http://doi.org/10.1039/c0pp00155d>
- 673 [26] R. Dillert, J. Stotzner, A. Engel, D.W. Bahnemann, Influence of inlet concentration and light
674 intensity on the photocatalytic oxidation of nitrogen(II) oxide at the surface of Aeroxide (R) TiO₂
675 P25, *J Hazard Mater*, 211 (2012) 240-246. <http://doi.org/10.1016/j.jhazmat.2011.11.041>
- 676 [27] A. Mills, C. Hill, P.K.J. Robertson, Overview of the current ISO tests for photocatalytic
677 materials, *J. Photochem. Photobiol. A-Chem.*, 237 (2012) 7-23.
678 <http://doi.org/10.1016/j.jphotochem.2012.02.024>
- 679 [28] C. Minero, A. Bedini, M. Minella, On the Standardization of the Photocatalytic Gas/Solid
680 Tests, *International Journal of Chemical Reactor Engineering*, 2013, pp. 717.
681 <https://doi.org/10.1515/ijcre-2012-0045>
- 682 [29] ISO Standard 22197-1:2016, Fine ceramics (advanced ceramics, advanced technical ceramics)
683 – test method for air-purification performance of semiconducting photocatalytic materials. , Part
684 1. Removal of nitric oxide. International Organization for Standardization, 2016.
685 <https://www.iso.org/standard/65416.html>
- 686 [30] A. Mills, S. Elouali, The nitric oxide ISO photocatalytic reactor system: Measurement of NO_x
687 removal activity and capacity, *J. Photochem. Photobiol. A-Chem.*, 305 (2015) 29-36.
688 <http://doi.org/10.1016/j.jphotochem.2015.03.002>

- 689 [31] S. Ifang, M. Gallus, S. Liedtke, R. Kurtenbach, P. Wiesen, J. Kleffmann, Standardization
690 methods for testing photo-catalytic air remediation materials: Problems and solution, Atmospheric
691 Environment, 91 (2014) 154-161. <http://dx.doi.org/10.1016/j.atmosenv.2014.04.001>
- 692 [32] S.K. Beaumont, R.J. Gustafson, R.M. Lambert, Heterogeneous Photochemistry Relevant to
693 the Troposphere: H₂O₂ Production during the Photochemical Reduction of NO₂ to HONO on UV-
694 Illuminated TiO₂ Surfaces, Chemphyschem, 10 (2009) 331-333.
695 <http://doi.org/10.1002/cphc.200800613>
- 696 [33] N. Bowering, G.S. Walker, P.G. Harrison, Photocatalytic decomposition and reduction
697 reactions of nitric oxide over Degussa P25, Applied Catalysis B: Environmental, 62 (2006) 208-
698 216. <https://doi.org/10.1016/j.apcatb.2005.07.014>
- 699 [34] R.J. Gustafsson, A. Orlov, P.T. Griffiths, R.A. Cox, R.M. Lambert, Reduction of NO₂ to
700 nitrous acid on illuminated titanium dioxide aerosol surfaces: implications for photocatalysis and
701 atmospheric chemistry, Chemical Communications, (2006) 3936-3938.
702 <http://doi.org/10.1039/b609005b>
- 703 [35] W. Lu, A.D. Olaitan, M.R. Brantley, B. Zekevat, D.A. Erdogan, E. Ozensoy, T. Solouki,
704 Photocatalytic conversion of nitric oxide on titanium dioxide: Cryotrapping of reaction products
705 for online monitoring by mass spectrometry, J. Phys. Chem. C, 120 (2016) 8056-8067.
706 <http://doi.org/10.1021/acs.jpcc.5b10631>
- 707 [36] M. Ndour, B. D'Anna, C. George, O. Ka, Y. Balkanski, J. Kleffmann, K. Stemmler, M.
708 Ammann, Photoenhanced uptake of NO₂ on mineral dust: Laboratory experiments and model
709 simulations, Geophysical Research Letters, 35 (2008). <http://doi.org/10.1029/2007gl032006>
- 710 [37] ASTM E1908-11. Standard Practice for Calculating Solar Reflectance Index of Horizontal
711 and Low-Sloped Opaque Surfaces. ASTM International, West Conshohocken, PA,
712 (2001), <https://doi.org/10.1520/E1980-11>.
- 713 [38] J.K. Sikkema, S.K. Ong, J.E. Alleman, Photocatalytic concrete pavements: Laboratory
714 investigation of NO oxidation rate under varied environmental conditions, Construction and
715 Building Materials, 100 (2015) 305-314. <http://dx.doi.org/10.1016/j.conbuildmat.2015.10.005>

716 [39] C.J. Cros, A.L. Terpeluk, N.E. Crain, M.C.G. Juenger, R.L. Corsi, Influence of environmental
717 factors on removal of oxides of nitrogen by a photocatalytic coating, Journal of the Air & Waste
718 Management Association, 65 (2015) 937-947. <http://dx.doi.org/10.1080/10962247.2015.1040524>

719 [40] F. Bai, R.A.T. Gould, M.T.M. Anderson, Photocatalytic coating, US Patent, 8,993,471 B2
720 (2015) <https://patents.google.com/patent/US8993471B8993472/en>.

721 [41] J.L.M. Jacobs, Photocatalytic composition and method for preventing algae growth on
722 building materials, US Patent, 6,881,701 B2 (2005) <https://patents.google.com/patent/US6881701>.

723 [42] ASTM G154-12a. Standard practice for operating fluorescent ultraviolet (UV) lamp apparatus
724 for exposure of nonmetallic materials. ASTM International, West Conshohocken, PA. (2012).
725 <https://doi.org/10.1520/G0154-12A>.

726 [43] Q-Lab, Q-Lab weathering research service. Florida - Arizona - Natural - Accelerated,
727 <https://www.q-lab.com/documents/public/a22e6272-737d-4e26-9bd9-d0ecc0bc2c20.pdf>, (2008).

728 [44] L. Sivachandiran, F. Thevenet, P. Gravejat, A. Rousseau, Investigation of NO and NO₂
729 adsorption mechanisms on TiO₂ at room temperature, Applied Catalysis B: Environmental, 142-
730 143 (2013) 196-204. <http://doi.org/10.1016/j.apcatb.2013.04.073>

731 [45] M. Ndour, P. Conchon, B. D'Anna, O. Ka, C. George, Photochemistry of mineral dust surface
732 as a potential atmospheric renoxification process, Geophysical Research Letters, 36 (2009)
733 L05816. <http://doi.org/10.1029/2008GL036662>

734 [46] O. Rosseler, M. Sleiman, V.N. Montesinos, A. Shavorskiy, V. Keller, N. Keller, M.I. Litter,
735 H. Bluhm, M. Salmeron, H. Destailats, Chemistry of NO_x on TiO₂ surfaces studied by ambient
736 pressure XPS: products, effect of UV irradiation, water, and coadsorbed K⁺, J. Phys. Chem. Lett.,
737 4 (2013) 536-541. <http://doi.org/10.1021/jz302119g>

738 [47] L. Sivachandiran, F. Thevenet, A. Rousseau, D. Bianchi, NO₂ adsorption mechanism on TiO₂:
739 An in-situ transmission infrared spectroscopy study, Applied Catalysis B: Environmental, 198
740 (2016) 411-419. <http://dx.doi.org/10.1016/j.apcatb.2016.05.065>

741 [48] L. Cao, Z. Gao, S.L. Suib, T.N. Obee, S.O. Hay, J.D. Freihaut, Photocatalytic Oxidation of
742 Toluene on Nanoscale TiO₂ Catalysts: Studies of Deactivation and Regeneration, Journal of
743 Catalysis, 196 (2000) 253-261. <https://doi.org/10.1006/jcat.2000.3050>

744 [49] M.K. Chemweno, L.G. Cernohlavek, W.A. Jacoby, Deactivation of titanium dioxide
745 photocatalyst by oxidation of polydimethylsiloxane and silicon sealant off-gas in a recirculating
746 batch reactor, J. Air & Waste Manag. Assoc., 58 (2008) 12-18. [http://dx.doi.org/10.3155/1047-](http://dx.doi.org/10.3155/1047-3289.58.1.12)
747 [3289.58.1.12](http://dx.doi.org/10.3155/1047-3289.58.1.12)

748 [50] S.O. Hay, T.N. Obee, C. Thibaud-Erkey, The deactivation of photocatalytic based air purifiers
749 by ambient siloxanes, Applied Catalysis B: Environmental, 99 (2010) 435-441.
750 <http://doi.org/10.1016/j.apcatb.2010.06.018>

751

SUPPORTING INFORMATION

De-pollution efficacy of photocatalytic roofing granules

Xiaochen Tang¹, Lara Ughetta², Simon K. Shannon², Sébastien Houzé de l'Aulnoit¹, Sharon Chen¹, Rachael A. T. Gould², Marion L. Russell¹, Jiachen Zhang³, George Ban-Weiss³, Rebecca L. A. Everman², Frank W. Klink², Ronnen Levinson¹, Hugo Destailats^{1,*}

1. Heat Island Group, Lawrence Berkeley National Laboratory, 1 Cyclotron Road, Berkeley, California 94720.
2. Industrial Mineral Products Division, The 3M Company, 3M Center, Building 209, 01-W-14, St. Paul, Minnesota 55144.
3. Department of Civil and Environmental Engineering, University of Southern California, Los Angeles, California 90089, USA.

* Corresponding author E-mail: HDestailats@lbl.gov

Note S1: Broadband UV irradiance from UVA-340 lamp in weathering apparatus

The broadband UV irradiance (also known as “total ultraviolet”, or TUV) delivered by the UVA-340 lamp in the commercial weathering apparatus (Model QUV/Spray with Solar Eye Irradiance Control, Q-Lab) when operated in accordance with Cycle 1 of ASTM Standard G154-12a “Standard Practice for Operating Fluorescent Ultraviolet (UV) Lamp Apparatus for Exposure of Nonmetallic Materials”¹ was computed by

- a. digitizing the spectral irradiance labeled “UVA-340” in Figure 11 of Q-Lab Technical Bulletin LU-0822 “Sunlight, Weathering & Light Stability Testing”;²
- b. scaling this spectral irradiance to attain the value of $0.89 \text{ W m}^{-2} \text{ nm}^{-1}$ at 340 nm specified by ASTM G154-12a, Cycle 1; and
- c. integrating the scaled irradiance from 295 to 400 nm.

The resulting broadband UV irradiance was 48.0 W m^{-2} , or 173 kJ m^{-2} per hour of lamp operation. Note that the lamp is on 8 h and off 4 h in each 12-h cycle.

¹ ASTM G154-12a, Standard practice for operating fluorescent ultraviolet (UV) lamp apparatus for exposure of nonmetallic materials, ASTM International, West Conshohocken, PA, 2012. <https://doi.org/10.1520/G0154-12A>

² Technical Bulletin LU-0822, Sunlight, weathering & light stability testing. Q-Lab Corporation, Westlake, OH, 2011. <https://www.q-lab.com/documents/public/cd131122-c252-4142-86ce-5ba366a12759.pdf>

Table S1: Solar reflectance of shingle prototypes (Group A).

Sample ID	Average	Standard Deviation
A0	0.225	0.010
A1	0.167	0.006
A2	0.163	0.003
A3	0.118	0.007
A4	0.299	0.003
A5	0.287	0.006

The values reported in Table S1 represent the average of three measurements per specimen following ASTM C1549-16 “Standard Test Method for Determination of Solar Reflectance Near Ambient Temperature Using a Portable Solar Reflectometer”.³ We used a Solar Spectrum Reflectometer (Devices & Services; Dallas, Texas, version 6) with the air mass 1.5 beam-normal solar reflectance output “1.5E”, as specified by the ANSI/CRRC-1-2016 Standard.⁴

³ ASTM C1549-16, Standard test method for determination of solar reflectance near ambient temperature using a portable solar reflectometer. ASTM International, West Conshohocken, PA, 2016.
<https://doi.org/10.1520/C1549-16>

⁴ ANSI/CRRC-1-2016 Standard test methods for determining radiative properties of materials. American National Standards Institute / Cool Roof Rating Council, 2016.
<http://coolroofs.org/product-rating/ansi-crrc-s100>



Figure S1: (A) Shingle specimen and (B) loose granules spread evenly inside the exposure chamber.



Figure S2: Rack used for natural exposure in Berkeley, CA.

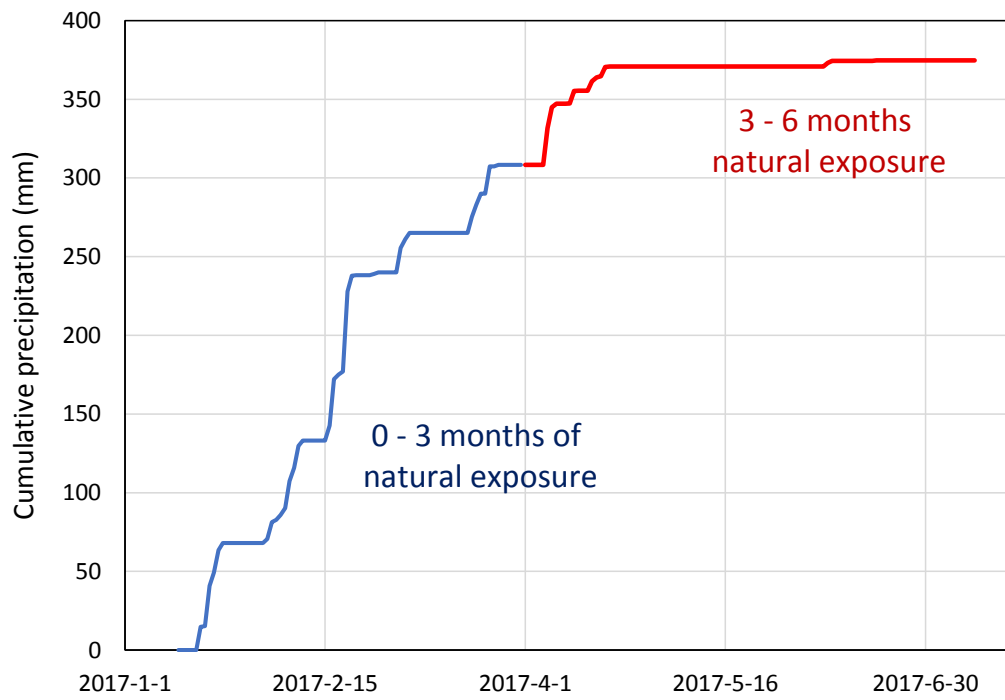


Figure S3: Cumulative precipitation in Berkeley, CA, during the six-month exposure period for samples A4 and A5.

Table S2: Hourly average solar irradiance ($W\ m^{-2}$) measured at the California Irrigation Management Information System (CIMIS) Station 213 in El Cerrito, CA.

Hour of day*	Average solar irradiance 2016-03-25 to 2016-07-11	Average solar irradiance 2017-01-13 to 2017-07-11
1	0	0
2	0	0
3	0	0
4	0	0
5	0.6	0.3
6	17	8.6
7	118	69
8	267	164
9	424	291
10	577	405
11	718	496
12	798	547
13	831	559
14	796	544
15	705	472
16	563	374
17	389	251
18	212	127
19	65	39
20	3.4	2.1
21	0	0
22	0	0
23	0	0
24	0	0

* For example, hour of day 1 = 0:00 - 1:00.

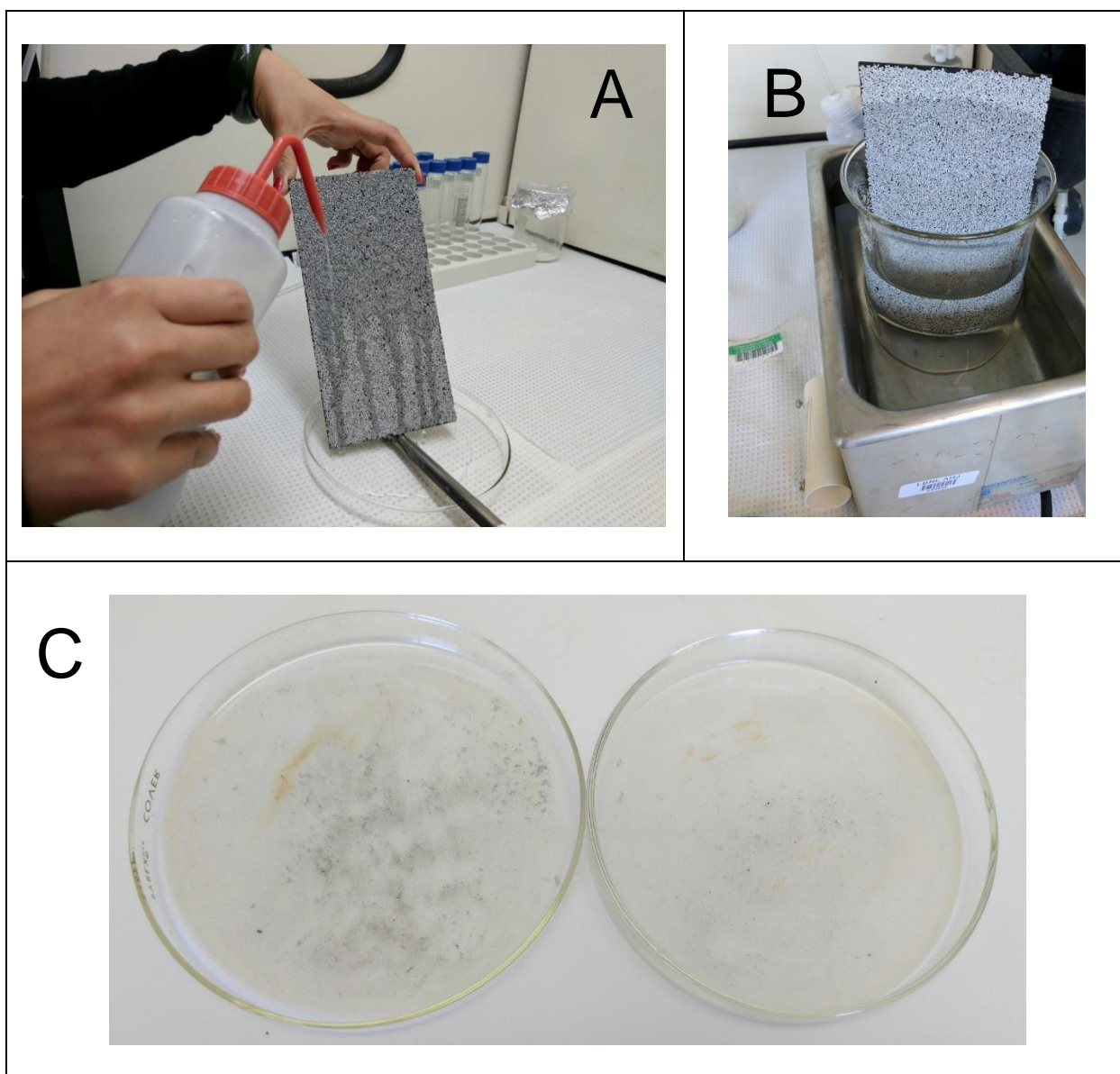


Figure S4: Laboratory cleaning operations applied to A4 and A5 specimens exposed for six months in Berkeley, CA. Images show (A) “soft cleaning” by rinsing; (B) “hard cleaning” using sonication; and (C) residues collected on petri dish during “soft cleaning”.

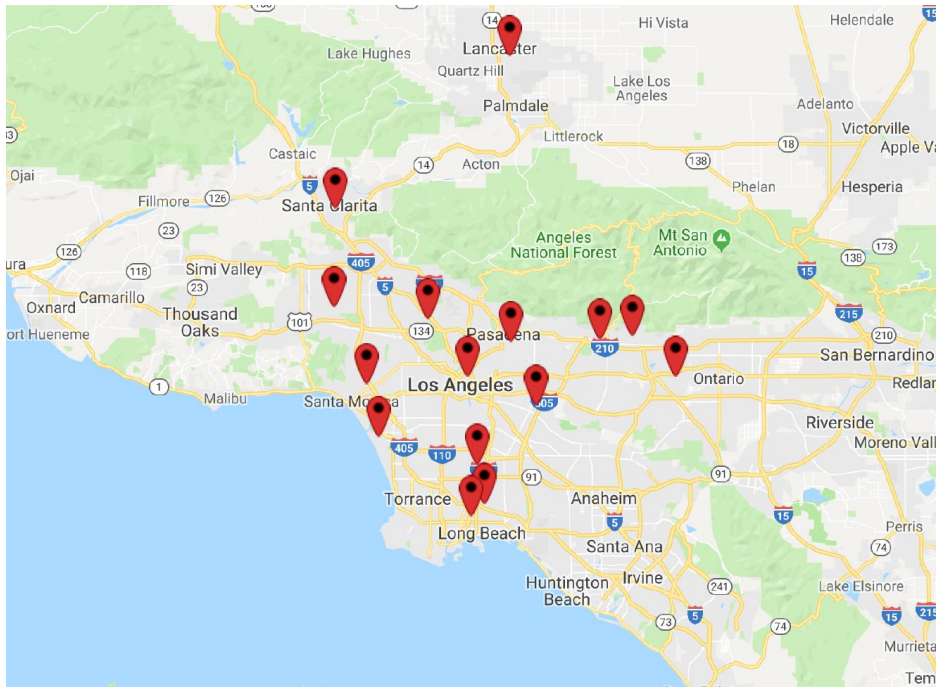
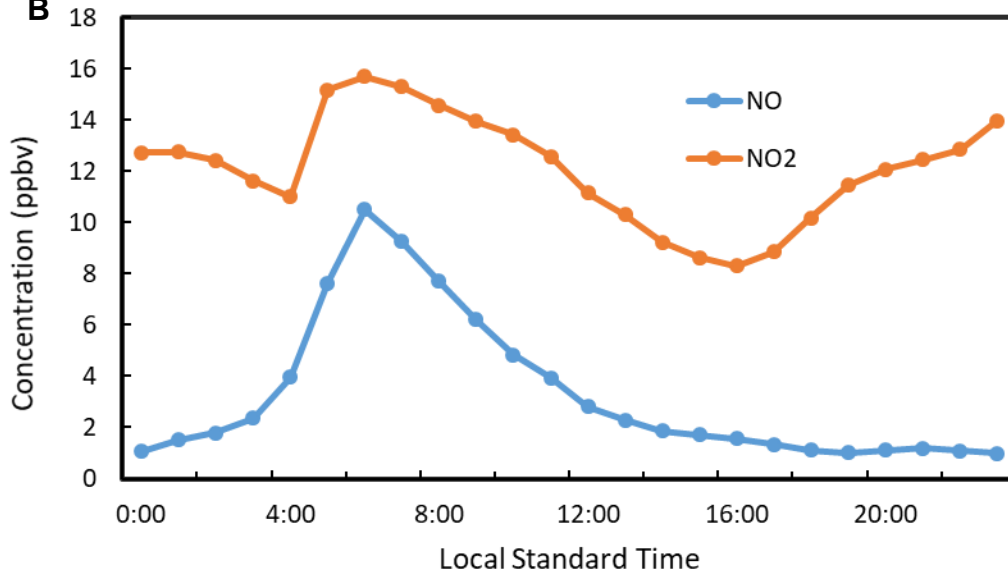
A**B**

Figure S5: Evaluation of NO/NO₂ mixing ratio in Los Angeles. (A) Map showing the 13 stations monitoring NO and NO₂ in Los Angeles County; (B) Diurnal cycles of NO and NO₂ concentrations averaged among the 13 monitoring stations in Los Angeles County for July 2012.

Records corresponding to NO and NO₂ concentrations for 13 monitoring stations in Los Angeles County were obtained from the EPA Air Quality System (AQS).⁵ AQS data are collected from local, state, and federal air quality control agencies. Figure S5-A shows the location of the stations used in our analysis. Figure S5-B shows the diurnal cycles of NO and NO₂ concentrations averaged over the stations in Los Angeles County for July 2012.

As shown in Table S3, the ratio of daytime (06:00 – 20:00 local standard time [LST]) average NO to NO₂ concentrations is calculated to be 0.29 (~0.3).

⁵ US Environmental Protection Agency (US EPA). Air Quality System (AQS), 2018.
<https://www.epa.gov/aqs>

Table S3. Average, maximum, and minimum values of NO and NO₂ concentrations and the ratio of hourly NO to NO₂ concentrations during daytime (06:00 – 20:00 LST). Values were averaged among 13 AQS monitoring stations (shown in Figure S4-A) in Los Angeles County for July 2012.

	NO (ppb)	NO₂ (ppb)	NO/NO₂ ratio
Average	3.8	11.7	0.29
Maximum	10.5	15.7	0.67
Minimum	1.0	8.3	0.09

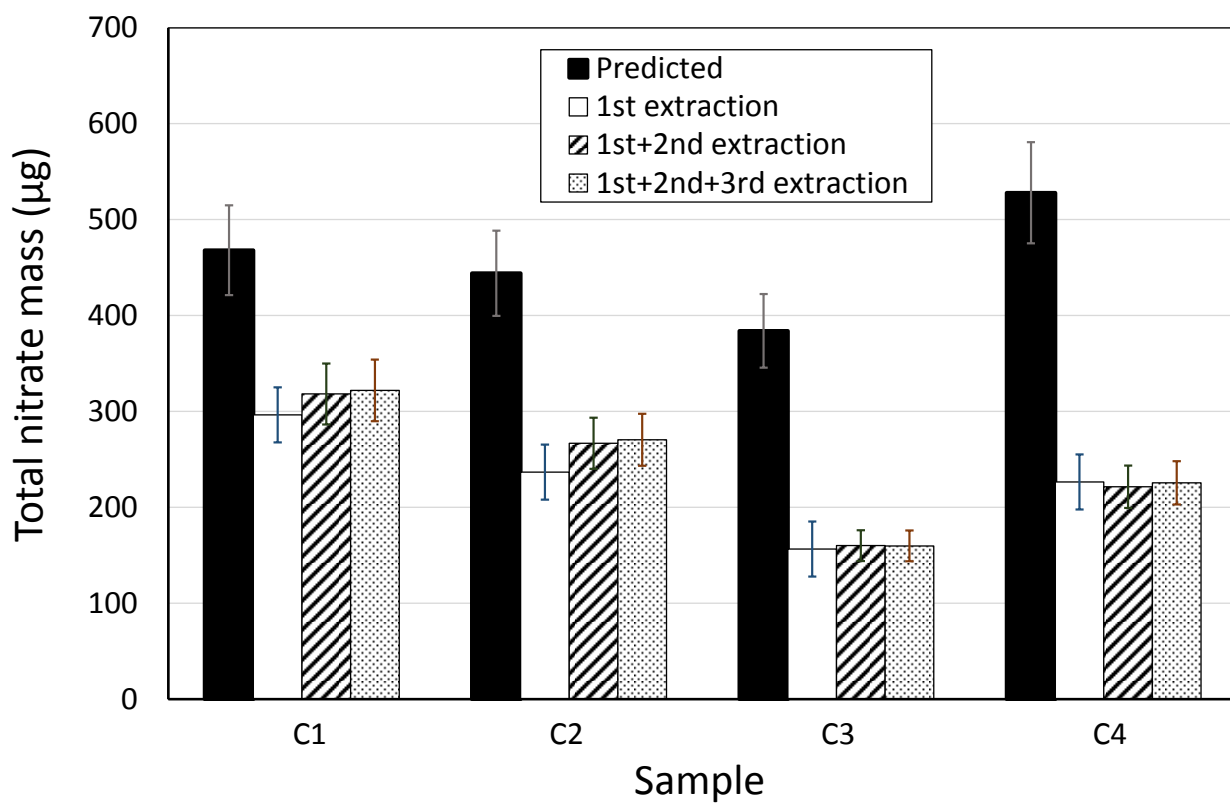


Figure S6: Comparison of the predicted mass of nitrate formed during the photocatalytic process and the amounts recovered with one, two and three sequential extraction of exposed granules.